On the Study of Electrorheological Properties of Polypyrrole-Silver Composite Particles of Various Conductivity

Subbu Annapandiyan

Master thesis
2013

Tomas Bata University in Zlín
Faculty of Technology

Tomas Bata University in Zlín
Faculty of Technology
Department of Polymer Engineering
Academic Year: 2012/2013

MASTER'S THESIS ASSIGNMENT

(PROJECT, ARTWORK, ARTISTIC PERFORMANCE)

Degree, First Name and Surname:	**Subbu Annapandiyan**
Personal Code:	**T11874**
Degree Programme:	**N2808 Chemistry and Materials Technology**
Degree Course:	**Polymer Engineering**
Thesis Topic:	**On the Study of Electrorheological Properties of Polypyrrole-Silver Composite Particles of Various Conductivity**

Thesis Guidelines:

Composites of conducting polymers and noble metals attract a large interest due to the variety of nanostructures displayed by both components. The combination of metallic and semiconductor types of conduction may provide materials having a reduced dependence of conductivity on temperature and this feature can be promising in the use of such particles as a disperse phase in electrorheological fluids, i.e. systems which are able to reversibly change their rheological properties according to the external electric field strength. The diploma thesis will deal with oxidation of pyrrole with mixture of two oxidants, ammonium peroxydisulfate and silver nitrate, to give polypyrrole?silver composites with variable content of silver in the composite and thus variable conductivity of prepared particles. Furthermore, the electrorheological characteristics of suspensions based on composite particles with optimum conductivity will be investigated.

1. Make a literature review on the given topic
2. Prepare polypyrrole particles of different conductivities depending on the content of silver
3. Measure dielectric, electric and rheological properties of suspensions based on particles of suitable conductivities
4. Evaluate and interpret obtained results

Thesis Extent:

Appendices:

Form of Thesis Elaboration: **printed/electronic**

Bibliography:

1. T. Hao, Electrorheological fluids: The non aqueous suspensions, 1st ed., Cambridge, Massachusetts, 2005, ISBN-13: 978-0-444-52180-4
2. Online databases accessible from TBU in Zlín

Thesis Supervisor:	**Ing. Michal Sedlačík**
Date Assigned:	**11 February 2013**
Thesis Due:	**17 May 2013**

Zlín, 11 February 2013

L.S.

doc. Ing. Roman Čermák, Ph.D.
Dean

doc. Ing. Roman Čermák, Ph.D.
Head of Department

Master Thesis Author Statement

I hereby acknowledge that:

- Upon final submission of my Thesis, I agree with its publishing in accordance with Act No. 111/1998 Coll., on Higher Education Institutions and on Amendment and Supplement to Some Other Acts, (The Higher Education Act), without regard to the defence result;
- I approve of the release of my Master Thesis in electronic form on the university information system, accessible for reading only;
- To my Master Thesis fully applies Act No. 121/2000 Coll., on Author Proprietary Rights, as well as the Modification and Amendment of Other Acts (Author Proprietary Rights Act), connected to author's proprietary rights and their changes in later versions of legal directives, esp. Section 35 Para 3;
- In accordance with Section 60 Para 1 of the Author Proprietary Rights Act, TBU in Zlin is entitled to enter into a licence agreement about the use of the Thesis to the extent defined in Section 12 Para 4 of the Author Proprietary Rights Act;
- In accordance with Section 60 Para 2 and 3, I can use my Master Thesis, or render the licence to its use, only with the prior expressed written agreement of TBU in Zlín, which is in such case entitled to require from me appropriate financial compensation to cover the cost of creating the Master Thesis (up to the total sum);
- If the software provided by TBU or other entities was used only for study and research (non-commercial) purposes in the development of the Master Thesis, it is not possible to use the Master Thesis commercially.

I herewith declare that:

- The contents of the file handed over are identical with the printed copies;
- I have created this Master Thesis on my own and cited all used sources. In case the results are published, I shall be cited as author.

In Zlín .....

Date: 16/5/2013

.....

signature

Note: Relevant Czech legislation applied.

.

Dedicated to the greatness of visionary inventor NIKOLA TESLA

ABSTRAKT

Tato diplomová práce je zaměřena na přípravu kompozitních částic polypyrol-stříbro (PPy-Ag) a srovnání jejich chemických vlastností a elektroreologických (ER) a dielektrických vlastností v suspenzích v silikonovém oleji se samotnými PPy částicemi. Kompozitní částice PPy-Ag byly připraveny pomocí oxidace pyrolu směsí persíranu amonného a dusičnanu stříbrného. Experimenty ukázaly, že ačkoliv přítomnost Ag zvýšila vodivost o jeden řád, ER účinnost těchto částic nebyla ve srovnání s čistým PPy výrazně ovlivněna při nižších intenzitách elektrického pole. Přítomnost Ag v částicích navíc zvýšila jejich vzájemnou kompatibilitu se silikonovým olejem a urychlila mezifázovou polarizaci kompozitních částic PPy-Ag.

Klíčová slova: polypyrol, stříbro, APS, $AgNo_3$, kompozit, elektroreologie, dielektrická spektroskopie.

ABSTRACT

This Master Thesis is aimed on the synthesis of polypyrrole-silver (PPy-Ag) composite particles and comparing their chemical, electrorheological (ER) and dielectric properties of their suspensions in silicone oil with those of pure PPy particles. Polypyrrole-silver composite particles were synthesized by oxidation of Pyrrole with mixture of Ammonium persulfate and Silver nitrate. Although the presence of Ag in the composite particles increased their conductivity in one order of magnitude, Experiments revealed that the ER performance did not change significantly at low electric field strengths compared to that of pure PPy. Moreover, it appeared that Ag improved the compatibility of dispersed particles with silicone oil used as a carrier liquid in ER suspensions and caused faster interfacial polarization of PPy-Ag composite particles.

Keywords: Polypyrrole, Silver, APS, $AgNO_3$ composite particles, electrorheology, dielectric spectroscopy.

ACKNOWLEDGEMENTS

I would like to express my deepest gratitude to my supervisor Dr. Michal Sedlacik for his guidance, understanding, support, criticism, encouragements and valuable discussions throughout my thesis. I also wish to thank my friend Tomas Plachy for his support and help during my experiments.

CONTENTS

INTRODUCTION **10**
THEORY **11**
1 CONDUCTIVE POLYMERS **12**
1.1 MODIFICATION OF CONDUCTIVITY BY DOPING **13**
1.2 POLYPYRROLE **14**
1.2.1 SYNTHESIS AND STRUCTURE OF POLYPYRROLE 14
1.2.2 ELECTRONIC CONDUCTION IN POLYPYRROLE 17
1.3 USES OF CONDUCTIVE POLYMERS **18**
2 ELECTRORHEOLOGICAL EFFECT **19**
2.1 ELECTRORHEOLOGICAL FLUIDS **19**
2.2 TYPES OF ELECTRORHEOLOGICAL EFFECTS **21**
2.2.1 POSITIVE AND NEGATIVE ER EFFECT 21
2.2.2 PHOTO ER EFFECT 24
2.2.3 MAGNETORHEOLOGICAL EFFECT 25
2.3 FACTORS WHICH AFFECT ER EFFECT **26**
2.3.1 EFFECT OF ELECTRIC FIELD STRENGTH 26
2.3.2 EFFECT OF ELECTRIC FIELD FREQUENCY 28
2.3.3 EFFECT OF PARTICLE CONCENTRATION 29
2.3.4 EFFECT OF TEMPERATURE 30
2.3.5 EFFECT OF PARTICLE DIELECTRIC PROPERTIES 32
2.3.6 EFFECT OF THE CHOICE OF LIQUID MEDIUM 32
3 APPLICATIONS OF ER FLUIDS **33**
3.1 ER VALVES AND THEIR AUTOMOTIVE APPLICATIONS **33**
3.1.1 ER FLUID CONTROLLED DAMPERS 34
3.1.2 HYDRODYNAMIC CLUTCH 36
3.1.3 PADLESS ULTRAPRECISION POLISHING 37
3.1.4 REHABILITATION DEVICES 38
II ANALYSIS **39**
4 AIM OF WORK **40**
5 SYNTHESIS OF POLYPYRROLE – SILVER COMPOSTIES **41**
5.1 CHARACTERIZATION METHODS **44**
5.1.1 SEM, XRD, TGA AND FTIR ANALYSIS 44
5.1.2 CONDUCTIVITY MEASUREMENTS 44
5.1.3 ELECTRORHEOLOGICAL MEASUREMENTS 44
5.1.4 DIELECTRIC MEASUREMENTS 45

6 RESULTS AND DISCUSSIONS 46
6.1 MORPHOLOGY OF PPY & PPY-AG COMPOSITE PARTICLES 46
6.2 FTIR STUDIES ON THE SAMPLES 49
6.3 CHARACTERIZATION OF PPY AND PPY-AG PARTICLES 50
6.4 ELECTRORHEOLOGICAL MEASUREMENTS 52
6.4.1 THE EFFECT OF DEPROTONATION 59
6.4.2 EFFECT OF CHANGE IN PARTICLE VOLUME CONCENTRATION 60
6.4.3 DYNAMIC OSCILLATORY EXPERIMENTS 61
6.5 DIELECTRIC MEASUREMENTS 64
CONCLUSION 66
BIBLIOGRAPHY 67
LIST OF ABBREVIATIONS 73
LIST OF FIGURES 75
LIST OF TABLES 79

INTRODUCTION

Electrorheological (ER) suspensions, typically composed of polarizable particles in non-conducting carrier liquid are promising as the next generation smart fluids due to their ability to reversibly change their viscosity according to the applied external electric field.

In principle, the imposed electric field polarizes the dispersed particles which consequently join together resulting in the formation of chain-like structures along the direction of electric filed. These internal structures restrict the motion of the suspension and the system changes its state from liquid to solid-like leading to dramatic changes in their rheological properties [1]

The controllable and reversible changes of the rheological properties (viscosity, yield stress) is manifested macroscopically in the increased stiffness of ER suspensions which makes these materials a potential candidate in the fabrication of electric clutches or brakes, shock absorbers, valves and etc., [2]

Several kinds of materials can be used for the preparation of such ER suspensions, for example inorganic materials (such as TiO_2, $BaTiO_2$), organic materials (such as chitosan, alginate and its derivatives), and conducting polymers. In recent years conducting polymers have been widely used, due to their ease of preparation, less corrosive properties and their stability, compatibility with the carrier liquid. Polypyrrole (PPy) together with its derivatives either in particulate shape or fiber or shell material in core-shell structured particles represents one of the most promising conducting polymers in this field due to its simple synthesis, ease of alternation of their conductivity and thermal stability [3-6].

In this diploma thesis, incorporation of conducting Ag particles into PPy was adopted as new strategy for a possible method of controlling the conductivity of resulting particles, because conductivity of the particles is one of the most important parameters in the fabrication of ER suspensions. The incorporation of Ag was achieved via the oxidation of pyrrole using Silver nitrate ($AgNO_3$) and Ammonium persulfate (APS) as oxidants.

I. THEORY

1 CONDUCTIVE POLYMERS

Since 1977, the discovery of polymers which conduct electricity by Alan J. Heeger, Alan G. MacDiarmid and Hideki Shirakawa which eventually led them to win Nobel Prize for Chemistry in 2000, this new breed of polymers have opened a whole new concept in polymer science. Notable amount of research and development have been done so far exploiting this new phenomenon and finding new ways of utilizing it [7, 8].

The conducting polymers (CPs), also sometimes termed as conductive polymers or conjugated polymers are quite a different species in the sense that they conduct electricity intrinsically and they don't have any sort of conductive fillers as such. In recent years, polymers of heterocyclic compounds with adjacent (conjugated) double bonds have attracted most of the attention as the next generation '*smart materials*' [9].

Modification of the extended π- system of valence electrons along the conjugated backbone of these polymers renders it capable of conducting electricity [9]. This phenomenon is explained in detail later.

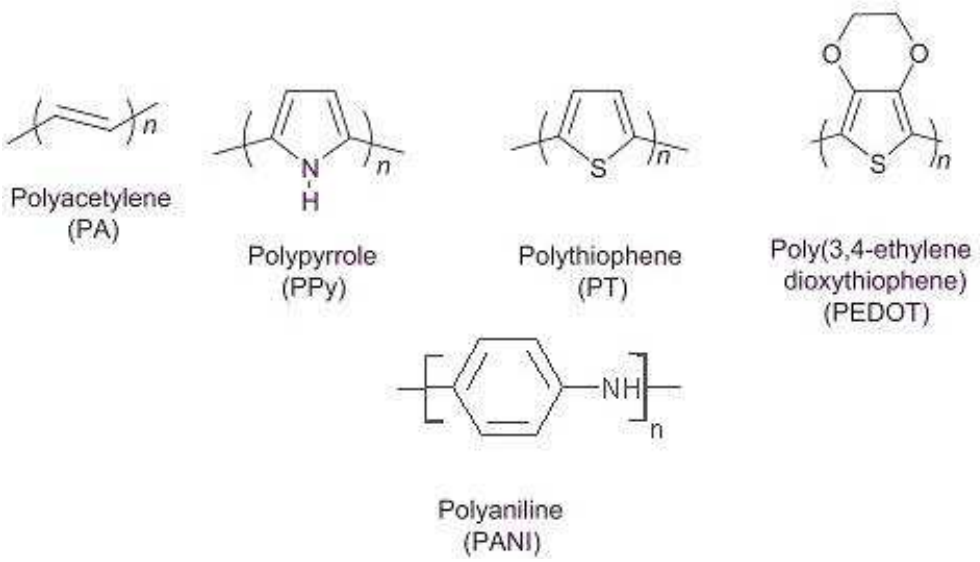

Figure 1: Structure of most common CPs and their abbreviations [9].

1.1 MODIFICATION OF CONDUCTIVITY BY DOPING

The Cps can be made conductive via a simple chemical oxidation or reduction, using a number of simple anionic or cationic species called “dopants”. The observed conductivity after the successful oxidation or reduction is due to the addition or removal of electron from the valence bond of the CPs which introduces charge centers on the polymer backbone [9, 10]. This process modification of conductivity of the CPs is known as doping.

Oxidation by a suitable dopant results in the generation of positively charged CP on the other hand the reduction process generates CP with a negatively charged backbone. For example P doping of PANi emeraldine base to is shown in Fig 2 [11].

Both *p*-type (electron accepting, e.g., PF_6, BF_4, AsF_6) and *n*-type (electron donating, e.g., Na, Li, Ca, Tetrabutylammonium) dopants can be used. The doping process is typically done by using vapours or solutions of the dopant or by electrochemical reactions. In certain situations, the polymer and the dopant are dissolved in the same solvent before forming the film or powder [11, 12].

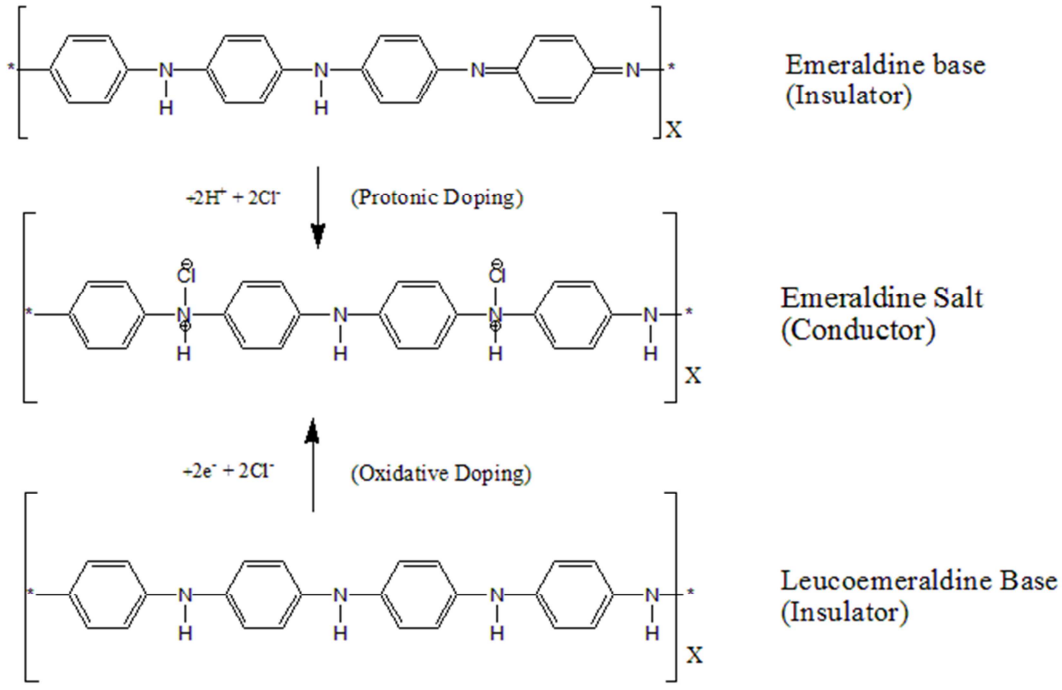

Figure 2: Illustration of the oxidative doping (p-doping) of Leucoemeraldine base and Emeraldine base results in the conductive Emeraldine salt [11].

1.2 POLYPYRROLE

Among the conducting polymers, polypyrrole (PPy) is especially encouraging for viable applications due to its good environmental stability, facile synthesis, higher conductivity, higher stability in oxidised state and the interesting redox properties than that of many other conducting polymers [6, 13]. PPy is basically an insulator; whereas it's oxidized derivatives (*p*-doped) are good electrical conductors. The conductivity mainly depends on the conditions and oxidative reagents used during the oxidation process. In practice PPy can't be *n*-doped, because *n*-doped PPy is not very stable as their *P*-doped variants. [9].

Polypyrrole is obtained as a black powder by the polymerization of pyrrole and has the repeating monomer units of pyrrole as its backbone which is illustrated in Fig 3.

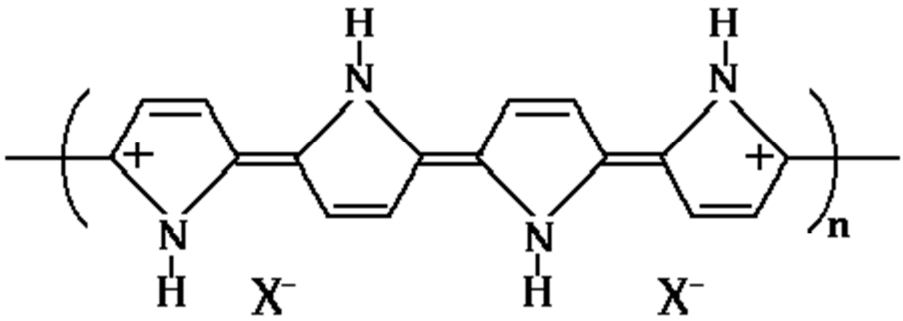

Figure 3: Structure of Polypyrrole [14].

1.2.1 SYNTHESIS AND STRUCTURE OF POLYPYRROLE

PPy is relatively easy to synthesis via electrochemical polymerization methods and their charge characteristics on the surface can certainly be altered by changing the dopant anion that is incorporated during the synthesis [15].

The chemical polymerization is carried out in the presence of various oxidants such as Ferric chloride ($FeCl_3$), Potassium per sulphate ($K_2S_2O_8$), and Ammonium persulfate $(NH_4)_2S_2O_8$ [16].

Different mechanisms were proposed to explain the pyrrole (Py) polymerization reaction. The mechanism (Fig 4) described by Kim and Song is often used in literatures is frequently used in the literature [17], where polymerization is initiated by the loss of two electrons and a proton from a pyrrole molecule forming the active intermediate. This intermediate species is then dimerized by a neutral Py molecule and the whole process is repeated until the polymerization reaction is completed [14, 15, 18].

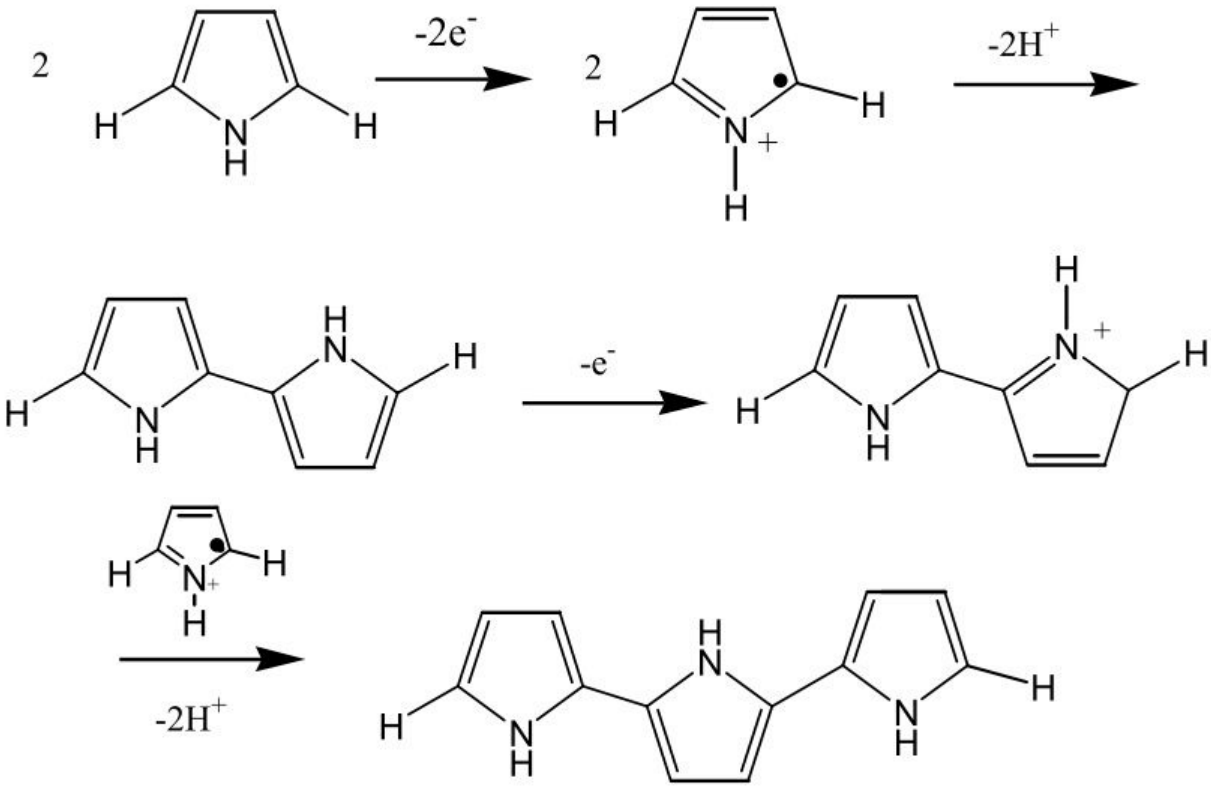

Figure 4: Oxidative polymerization of Py to PPy proceeds via the formation of a Py radical cation, which subsequently couples with another radical cation to form the Py dimer. This Process is then repeated to form longer chains [14].

PPy has resonance structures that resemble the aromatic or quinoid arrangements which are non-conductive which upon oxidation become conductive. The charge associated with the oxidized state is typically delocalised along the Py units and results in the formation of a radical cation or dication. The former is termed as a polaron and the latter is called bipolaron [14].

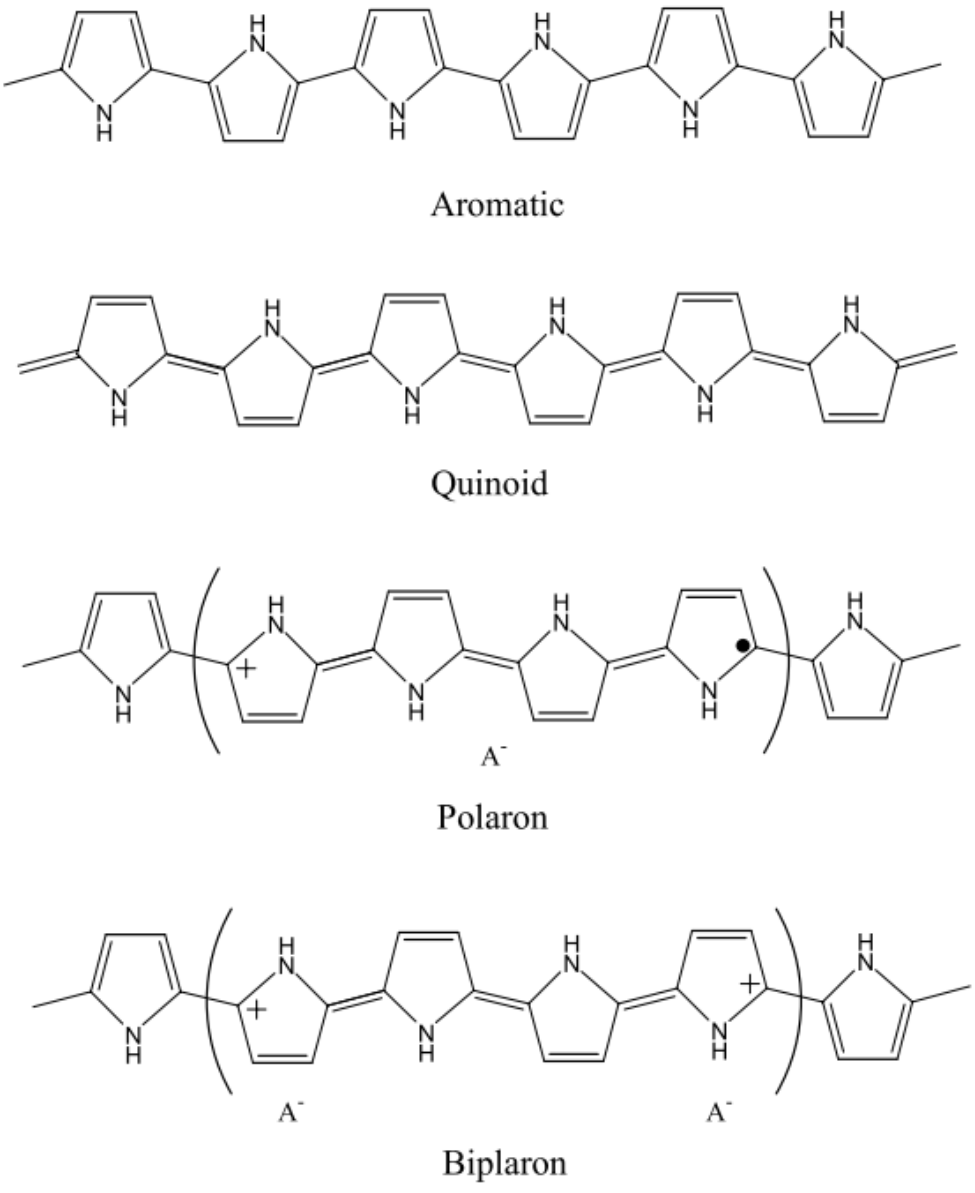

Figure 5: Illustration of the structures of neutral (Aromatic/quinoid) and the charged polaron/ bipolaron forms of PPy [14]

1.2.2 ELECTRONIC CONDUCTION IN POLYPYRROLE

The most important property of conducting polymers is their electrical conductivity. In PPy, the formation of polarons and bipolarons as a result of doping are considered to be the reason for the phenomenon of electrical transport. To explain the charge transport in PPy several electrical transport models have been proposed [19].

Hopping and Tunneling are considered to be the two fundamental types of charge transport in disordered materials or conducting polymers [20]. Mott's variable range hopping is the widely used model to explain the electronic conduction which is applicable for polypyrrole as well as for other conducting polymers [21].

The Pristine (undoped) PPy is a dielectric with the gap of 4 eV. Upon oxidation (doping), the gap reduces to ≤ 2.5 eV as a result of the removal of π-electrons from the upper level of the valence zone and renders the polymer as a semiconductor due to the formation of polarons and bipolarons. In chemical terms, the formation of a polaron is equivalent to the formation of a radical cation [22].

One should also note that excess oxidation (to the [monomer/oxidative agent] molar ratio) of polypyrrole results in the decreased electrical conductivity because it lowers the π-conjugation along the PPy chains. The Fig 6 explains the effect of change in concentration of monomer to the oxidative reagent on the conductivity of PPy [19].

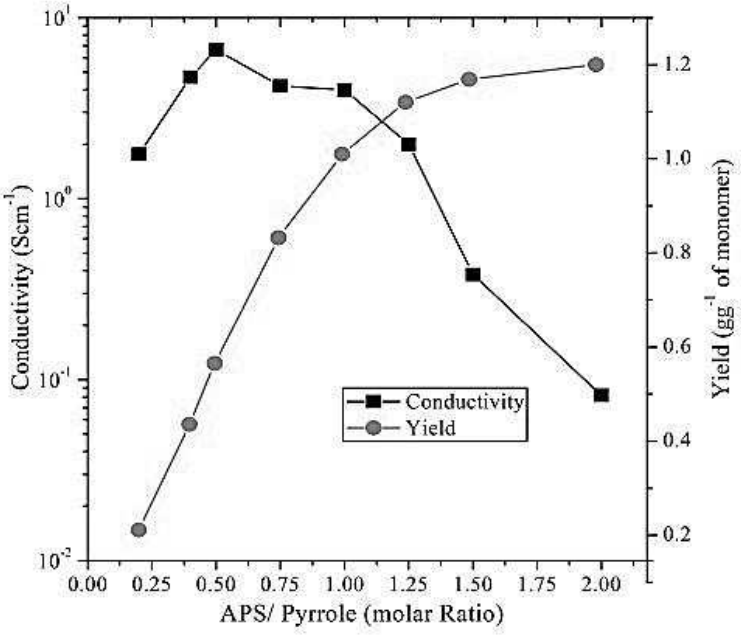

Figure 6 : Effect of monomer to oxidizing agent on the conductivity and yield. Note that the conductivity drops above the 1:1 molar ratio [19].

1.3 USES OF CONDUCTIVE POLYMERS

Owing to such interesting electrical properties the conducting polymers are extensively used in printing electronic circuits, organic solar cells, organic light-emitting diodes, supercapacitors, flexible transparent displays, radar-absorbing coating on stealth aircrafts, electromagnetic shielding, chemical and biosensors and in electrorheological systems [14, 23-26].

2 ELECTRORHEOLOGICAL EFFECT

The change in dynamic viscosity of a material (usually colloidal systems) when an external electric field is applied is termed as electrorheological effect (ER) effect.

This phenomenon was first reported in 1947 by Willis M. Winslow. Hence this ER effect is also sometimes called as '*Winslow effect*' [27, 28].

Since then it has kick started the investigation of different ER materials, their properties and ultimately of new commercial applications.

2.1 ELECTRORHEOLOGICAL FLUIDS

Over the last two decades a great deal of research has been done on the study of the properties, characterization and the commercial application of smart materials, which are engineered materials that have one or several properties that can be altered in a controlled manner by external stimuli such as the change in temperature, pH or applied electrical field, etc. Electrorheological (ER) fluids are the most fascinating among the smart materials [29, 30].

Electrorheological fluids are colloidal suspensions consist of particles (dispersed phase) with specific dielectric properties dispersed in an insulating oil (dispersion medium) such as silicone oil. The fascinating feature of the ER fluid is that, they can transform (or) solidify into a quasi-solid state almost immediately (within milliseconds) when subjected to an external electric field in the magnitude of a few kV/mm, which results in the increase in intrinsic viscosity abruptly. The even more fascinating fact is this liquid–solid transformation is reversible thereby the original flow state is recovered when the applied field is removed [30, 31]

The figs. 7 and 8 shows the changes in viscosity and sheer stress of ER fluid depending on the shear rate with and without the applied external electric field [32].

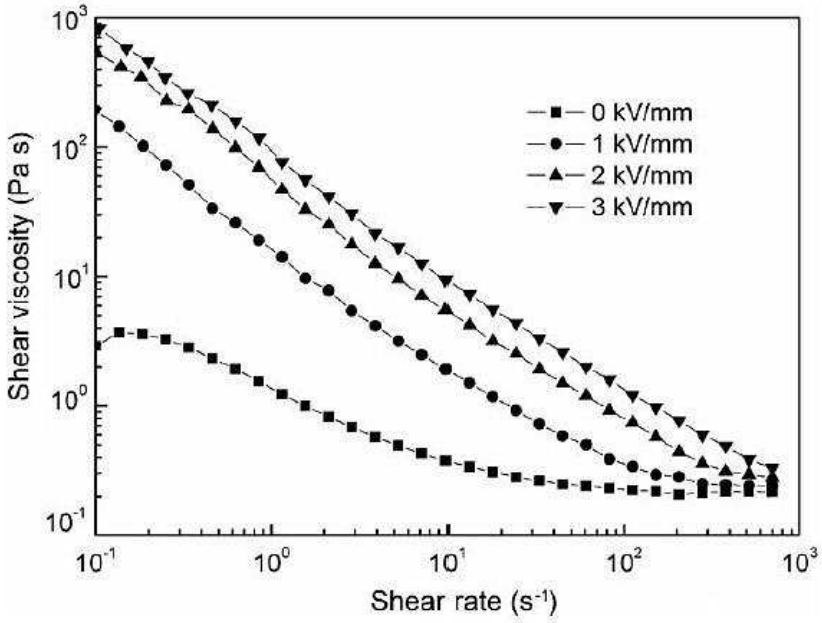

Figure 7: The change in viscosity of ER fluid (10 wt. % PPy–SBA-15 particles in silicone oil) at different applied electric field strengths [32].

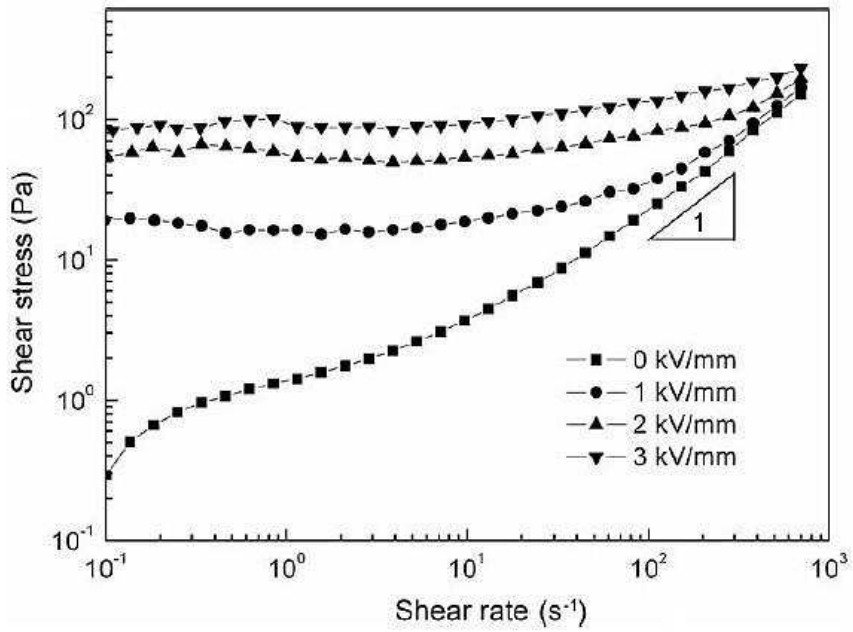

Figure 8: The change in Shear stress of ER fluid (10 wt. % PPy-SBA-15 particles in silicone oil) at different electric field strengths [32].

2.2 TYPES OF ELECTRORHEOLOGICAL EFFECTS

The smart fluids or suspensions can exhibit several types of ER effects. On the basis of changes in viscosity, shear stress and modulus they can be differentiated either as positive or negative ER effects [5, 33]. Whereas, based on the sensitivity or response of ER fluids on the type of applied external field they are classified as electro, magneto, electro-magneto rheological effect and photo effect [34].

2.2.1 POSITIVE AND NEGATIVE ER EFFECT

Positive ER effect results in the increase in viscosity and the relevant shear stress of ER fluid under the application of external electric field, the opposite is true in the case of materials which exhibit negative ER effect [35]. This dramatic increase in viscosity is due to the transformation from liquid to quasi-solid state which is caused by the aggregation of polarized particles into fibrous structures under an external electric filed. These structures restrict the motion of the fluid, under shear flow conditions these fibrous structures move intact along the shear direction which accounts for the increase in corresponding shear stress and viscosity [33, 36]. And it's worth stating that the positive ER effect is the most common ER phenomenon encountered in the literatures.

Formation of fibrous structures under the external electric field is shown in the Fig- 9.

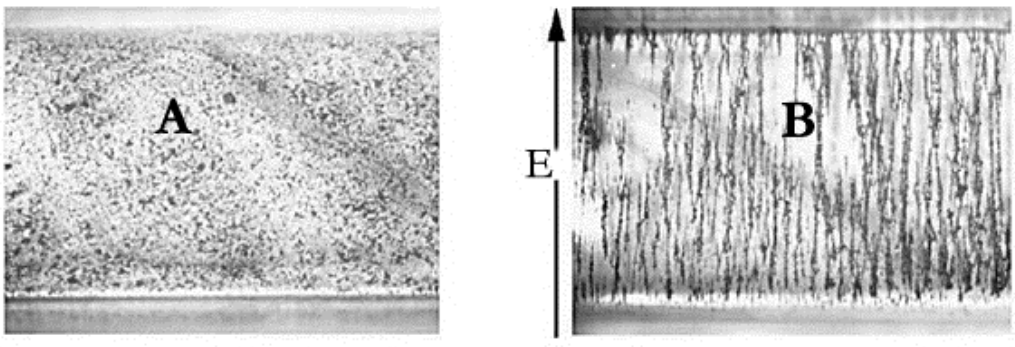

Figure 9: Suspension of dielectric particles (2 vol. %) in silicone oil, (A) The scattered random dispersed phase. (B) Formation of fibrous structures perpendicular to the field (The direction of the external field is indicated by the arrow) [33].

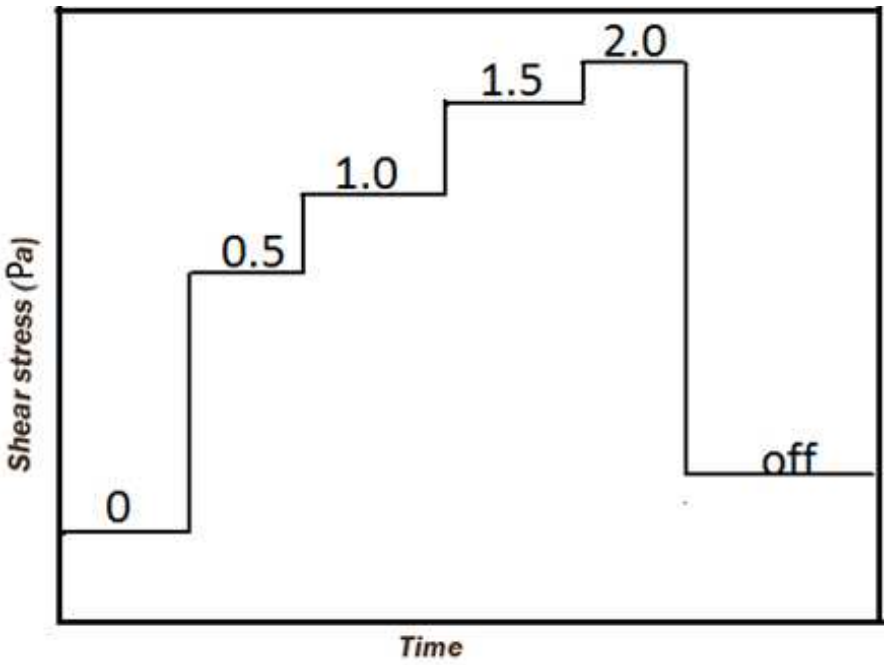

Figure 10: The change in shear stress of a positive ER fluid depending on the applied electric filed strength in kV/mm (indicated by the numbers on the each step [34].

This dramatic change in the rheological properties can be elucidated as follows; the application of electric filed induces dipoles on the dispersed particles. Later these dipoles are attracted to each other in a head-to-tail fashion thereby results in the formation of fibrous structures or aggregates which renders the suspension resisting flow (Fig-11). In order to make the suspension flowing along the direction of shear, these fibrous structures should be broken which results in the extra requirement of applied shear stress, hence the change in apparent viscosity of ER fluid [37, 38]

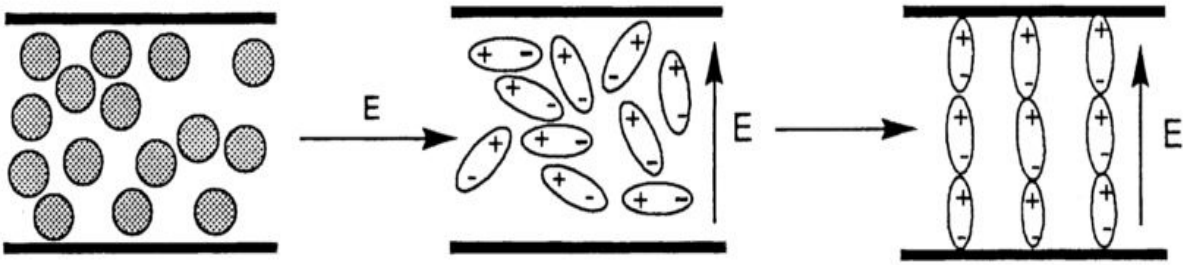

Figure 11 : Schematic illustration of the formation of dipoles and the resulting fibrous structures (head-to-tail orientation) perpendicular to the electric field [38].

It is obvious that the nature of the insulating fluid, particle shape, surface and dielectric properties are also the critical factors which determines the ER behavior of the ER fluids [39].

In the case of negative ER effect, the apparent viscosity of the suspension decrease as the applied external electric filed increases. In 1995, this phenomenon was first observed by Boissy and his co-workers in ER fluid of PMMA powder dispersed in silicone oil [40]. Two reasons are reported to explain the decrease in rheological properties.

1. Due to electrophoresis the particles migrate to one of the electrode under the applied electric field which leads to phase separation [35].
2. Quincke rotation – Accumulation of charges on the particle surface after the polarization under applied electric field as shown in Fig. 12, the charges on the top and bottom of the particle surface have the same sign as that of the upper and lower electrodes, this makes the dispersion unstable and causes the particles to rotate under the electric field [41].

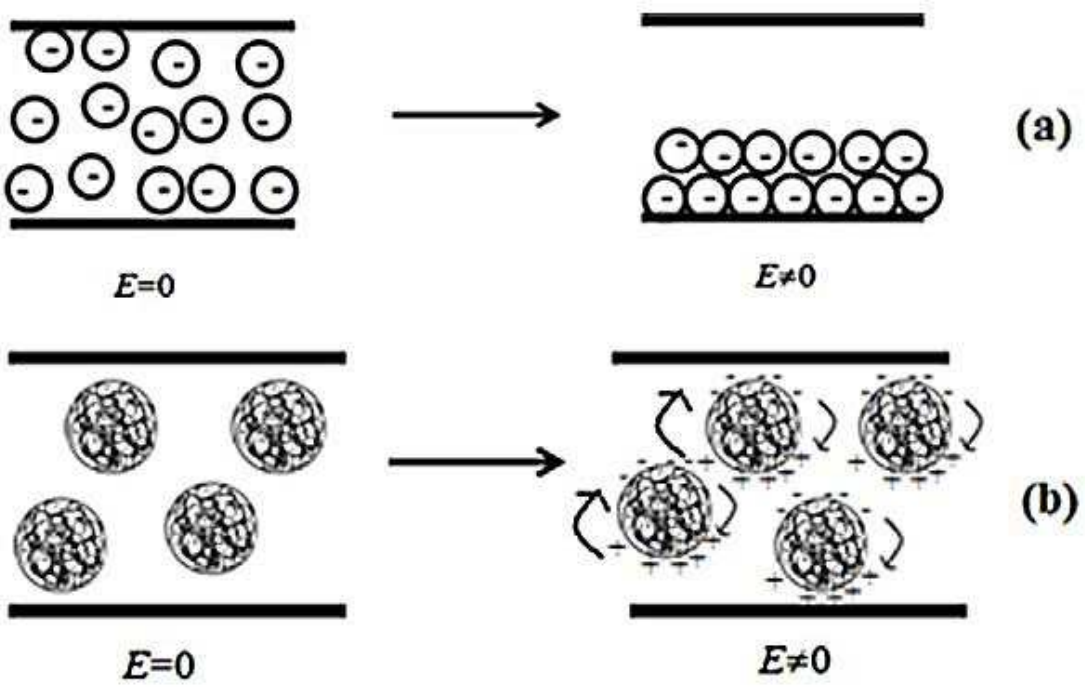

Figure 12: Illustration of (a) phase separation in the dispersion (b) Quincke rotation [41]

Several other systems were also found showing negative ER effect such as Teflon in silicone oil and polyindene /colemanite in silicone oil and etc., [41, 42]. The relationship between the positive and negative ER effect is shown graphically in Fig-13.

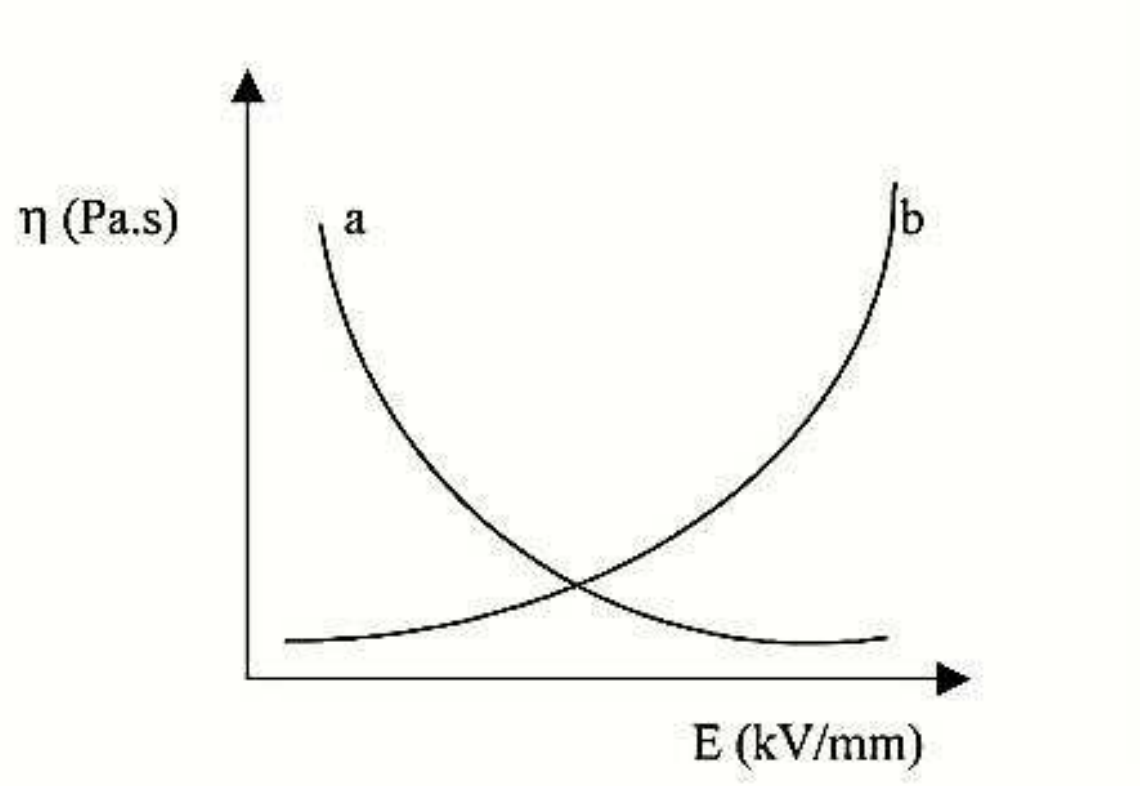

Figure 13: A- Negative ER effect and B- Positive ER effect, Note that the viscosity increases for A and decreases for B with respect to the increase in applied external electric field strength [34]

Both the positive and negative ER effects can be enhanced by UV illumination if the dispersed particles are photoactive [34, 38]. Titanium dioxide (TiO_2) in silicone oil is a perfect example in which the amount of water absorbed by the dispersed particles is a deciding factor i.e. the system exhibits positive ER effect when the amount of water is lower ($\leq$2 wt. %) where as a negative ER effect is observed when the water content is higher ($\geq$ 3 wt. %). Upon UV illumination, the formation of photo-generated carriers affect the electric conductivity of TiO_2 particles which accounts for the enhanced ER effect [43].

2.2.3 MAGNETORHEOLOGICAL EFFECT

Just as the ER effect, the magneto-rheological (MR) effect is defined as the reversible dramatic increase in rheological properties of MR suspensions induced by the applied external magnetic field strength. MR suspensions consists of ferromagnetic particles dispersed either in an insulating oil or conducting medium like water along with a suitable surfactant in order to prevent the particle sedimentation [44-46].

The application of magnetic field induces magnetic dipoles on the dispersed particles, which then align themselves to from the fibrous structure along the direction of the applied magnetic field which increments the viscosity over several order of magnitude [34].

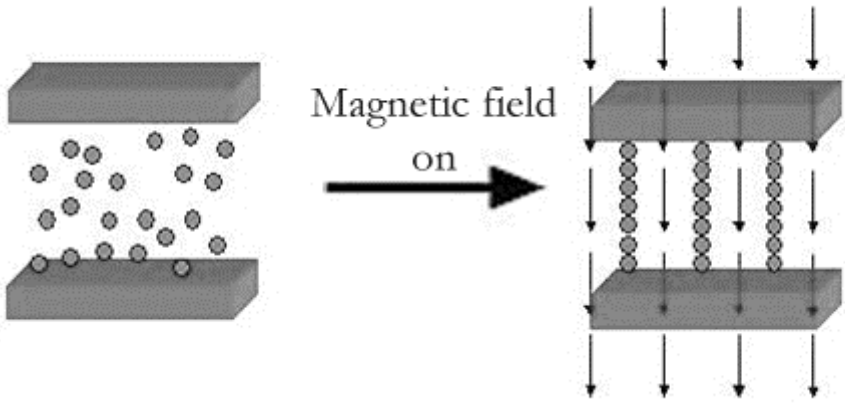

Figure 14: Formation of fibrillated particle structure under the magnetic field [60]

Basically the particles used to make MR suspensions cannot be used for ER systems because magnetic particles are more conductive; however the magnetic particles can be coated with an insulating agent, which renders the suspension applicable in both MR and ER systems. The combined effect of magnetic and electric field produces intensified rheological changes in the suspensions. This synergic effect is termed as electro-magneto-rheological effect [44, 47].

2.3 FACTORS WHICH AFFECT ER EFFECT

As mentioned above, there are several factors which affect the ER effect such as the electric field strength, frequency of the applied electric field, the dielectric properties, temperature, particle volume fraction or the electrode pattern.

2.3.1 EFFECT OF ELECTRIC FIELD STRENGTH

It has been found that every ER fluids has a definite critical electric field strength E_c, which is defined as the minimum strength of applied electric field at which the ER effect starts to build up, below which the ER is effect is not present [38].

The dependence of ER effect on the electric field strength can be expressed mathematically as [48].

$$E_c = \frac{\rho - c}{|\alpha|} \cdot \sqrt{\frac{8\pi k_B T}{c\rho \bar{v} \varepsilon_m}} \qquad (1)$$

Where ρ is the density of the dispersed particle, c is the particle concentration, $\bar{V}$ average volume of the particle, K_BT is the thermal energy, ε_m is the dielectric constant of the continuous phase, and the α is expressed as

$$\alpha = \frac{g}{g + \frac{\varepsilon_m}{(\varepsilon_p - \varepsilon_m)}} \qquad (2)$$

Where ε_p is the dielectric constant of the particles and g is the geometrical constant.

As depicted by the equation 1 it is evident that the critical electric field strength decreases as the particle concentration decreases.

The liquid to solid transformation of the ER fluid occurs when the applied electric field is just above ($\leq$) the E_c.

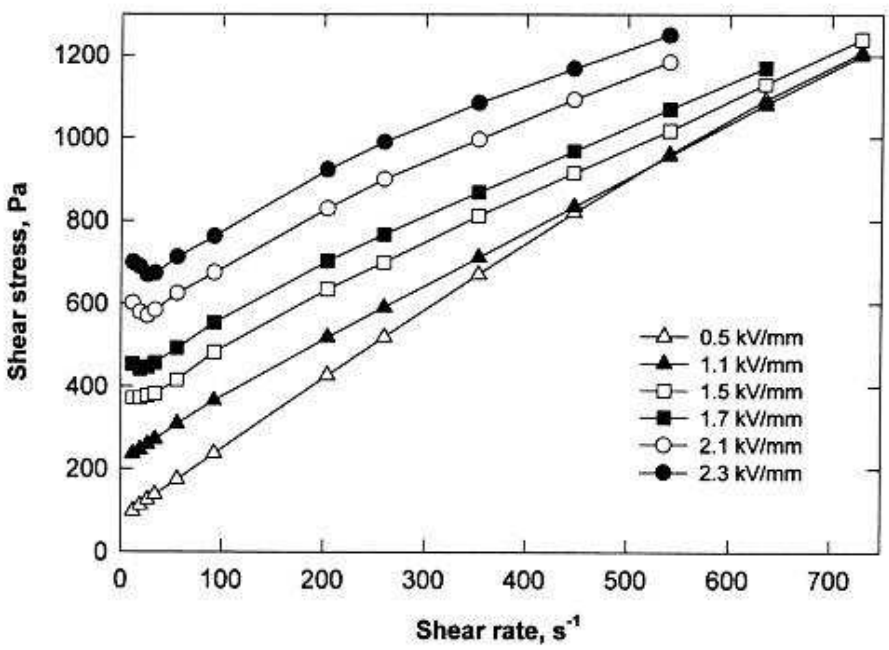

Figure 15: Dependence of the shear stress of ER fluid (PANi/Silicone oil) on the electric filed strength [61].

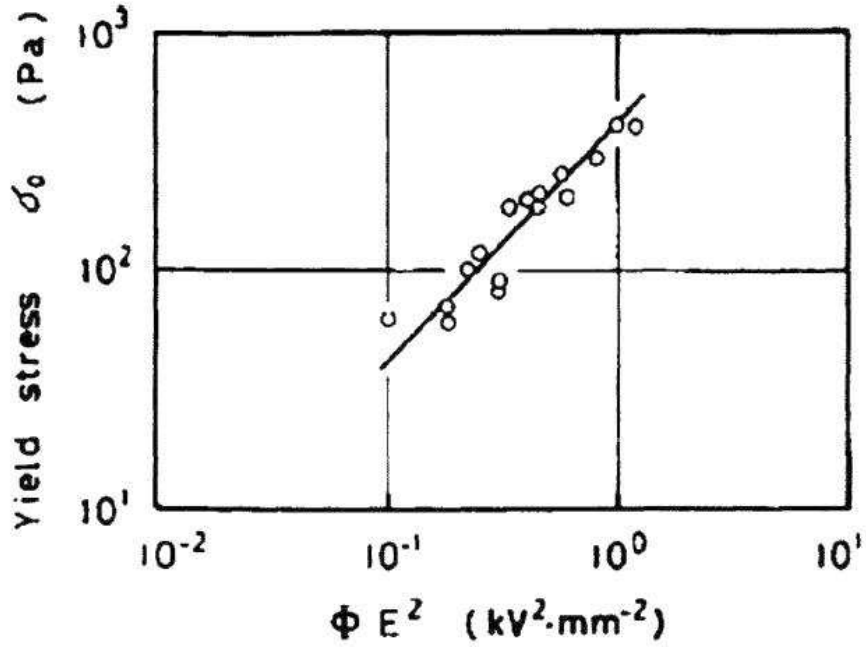

Figure 16: The change in yield stress of the ER system (silica/silicone oil) as a function of the square of applied electric field [62].

As sown in the Fig 16, it is evident that the shear stress is proportional to the square of the applied electric field $\tau \propto E^2$ *[62]*.

2.3.2 EFFECT OF ELECTRIC FIELD FREQUENCY

Frequency of the applied electric field also has an impact on the ER effect just as the electric field strength. As shown in the Fig. 17, the apparent viscosity of the ER fluid decreases as the frequency of the applied electric field increases, this was first noticed by Klass on the system consists of Silica/Silicone oil [38, 48].

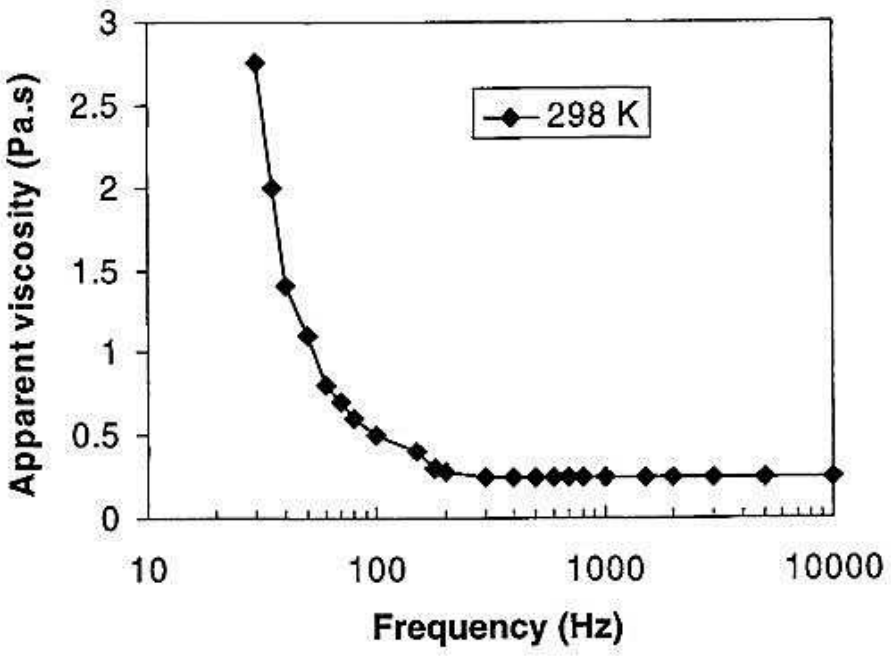

Figure 17: Decrease in apparent viscosity of the Silica/Silicone oil ER system with respect to the increase in frequency of the field [38]

This decrease in viscosity is due to the inability of the polarized particles to orient themselves along the field direction to form the fibrous structures at higher frequencies of the electric field. It is found that the decrease in yield stress is due to the decrease in dielectric constant of the ER fluid at higher frequency [38].

2.3.3 EFFECT OF PARTICLE CONCENTRATION

The particle volume concentration is another factor which affects the ER effect. Generally the yield stress is enhanced as the concentration (vol. %) of the particles in the system increases . The effect of particle volume fraction on the ER properties of ER fluid is shown in Fig. 18 [49].

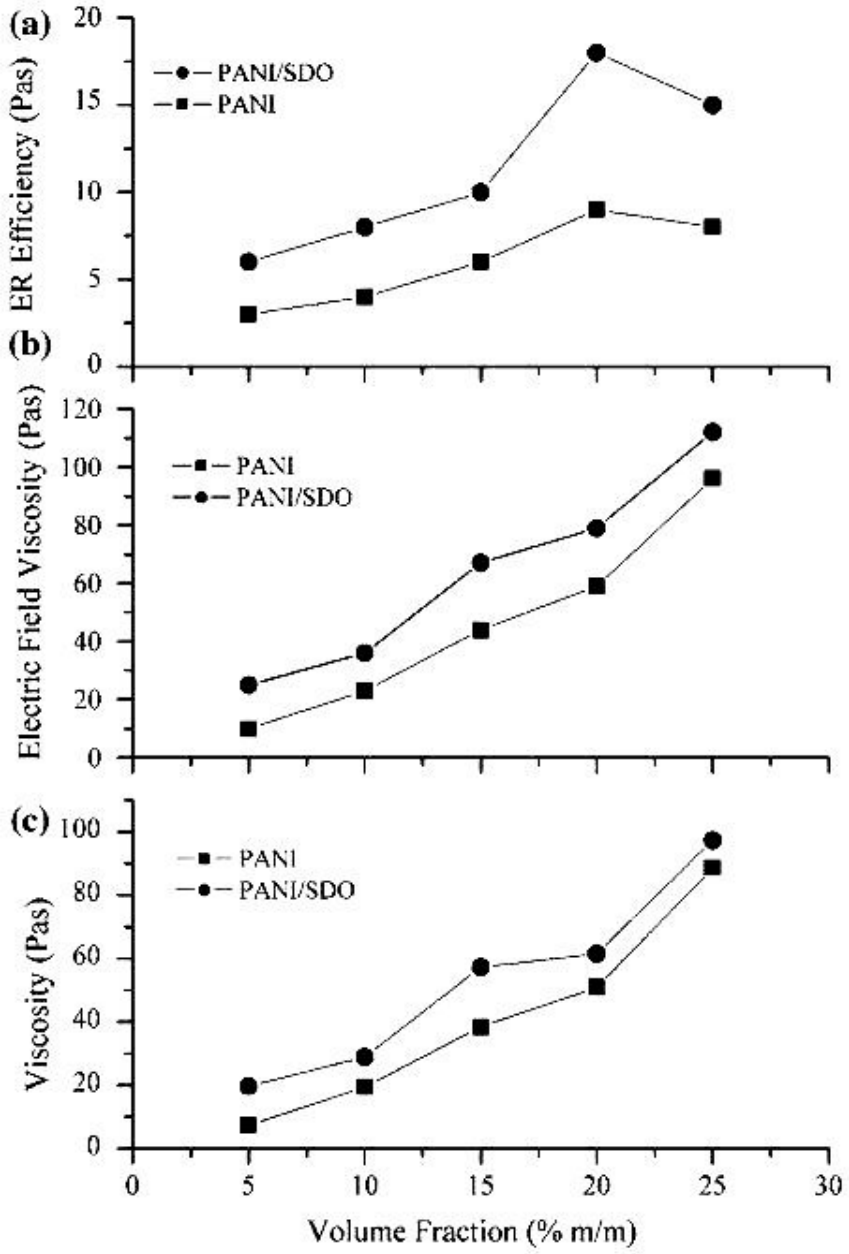

Figure 18 : Effect of change in concentration of particles on the ER properties of PANi in silicone oil and PANi in SiO_2 (SDO)

(E = 2 kV/mm, Shear rate 1.0 s^{-1}, T = 25 °C) [49].

2.3.4 EFFECT OF TEMPERATURE

Industrially applicable ER fluids should sustain wide range of operating temperature, since the change in temperature of the ER system could have definite effect on the ER activity. Temperature is a distinct factor which affects the particle polarizability, which is responsible for the dielectric properties of the ER fluids. Increase in temperature can cause the mobility of the charge carriers in the suspension which leads to an amplified ER effect.

On the other hand, the increase in temperature results in the increased thermal motion (Brownian movement), which hinders the polarized particles ability to form ordered structure under the applied electric field which results in decreased ER activity. Moreover increment in temperature reduces the overall viscosity (the particles are dispersed in oil medium) because the oil's viscosity is greatly reduced [38, 48, 49].

The two cases as described above are shown graphically in the Figs 19, 20 and 21.

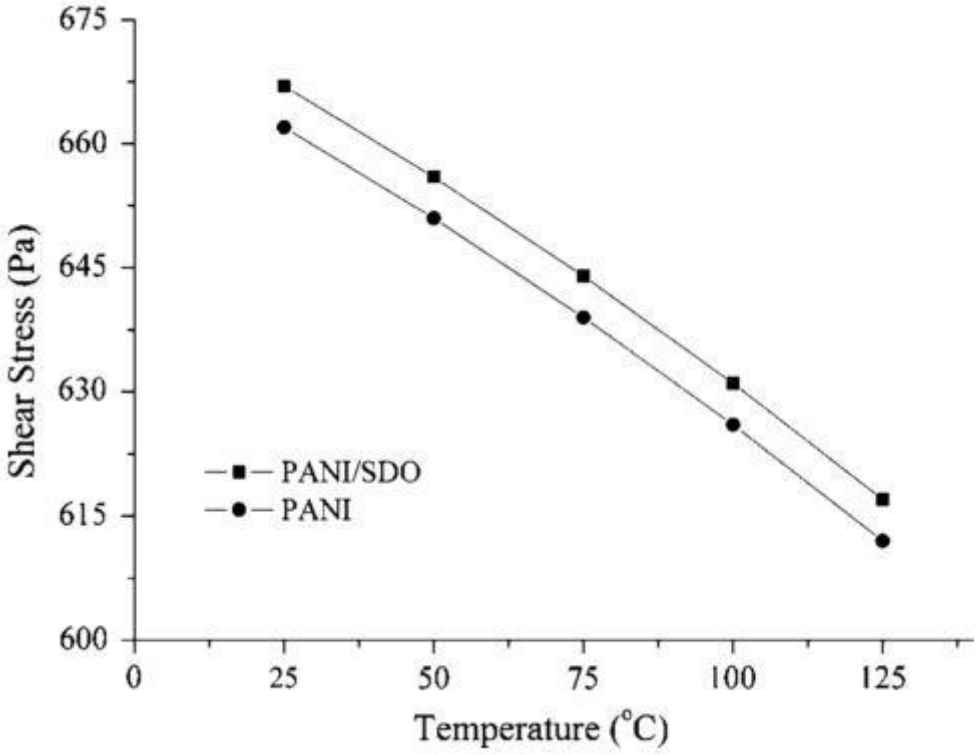

Figure 19: Negative Effect of Temperature on Shear stress of PANI/Silicone di oxide and PANi/Silicone oil ($\dot{\gamma}$ = 1.0 s^{-1}, 20 wt. %) *[49].*

Figure 19 shows the change in the shear stress of PANI/SO and PANI/SiO_2/SO suspensions under different temperatures at constant concentration (c = 20 wt. %). For this kind of ER colloids, the ER effect is a result of the polarization of dispersed particles when subjected to external electric field. Since the materials polarizability is temperature dependent, the shear stress of ER fluid is also subjective to the changes in temperature [45].

A decrease in shear stress with elevated temperature would be found in a suspension with the particle conductivity greater than the optimal value, while an increase would be found if the particle conductivity is less than the optimal value.

The positive effect of temperature is observed on the ER fluid of PANi derived carbonaceous nanotubes/Silicone oil, This is shown in the following Fig 20 and 21.

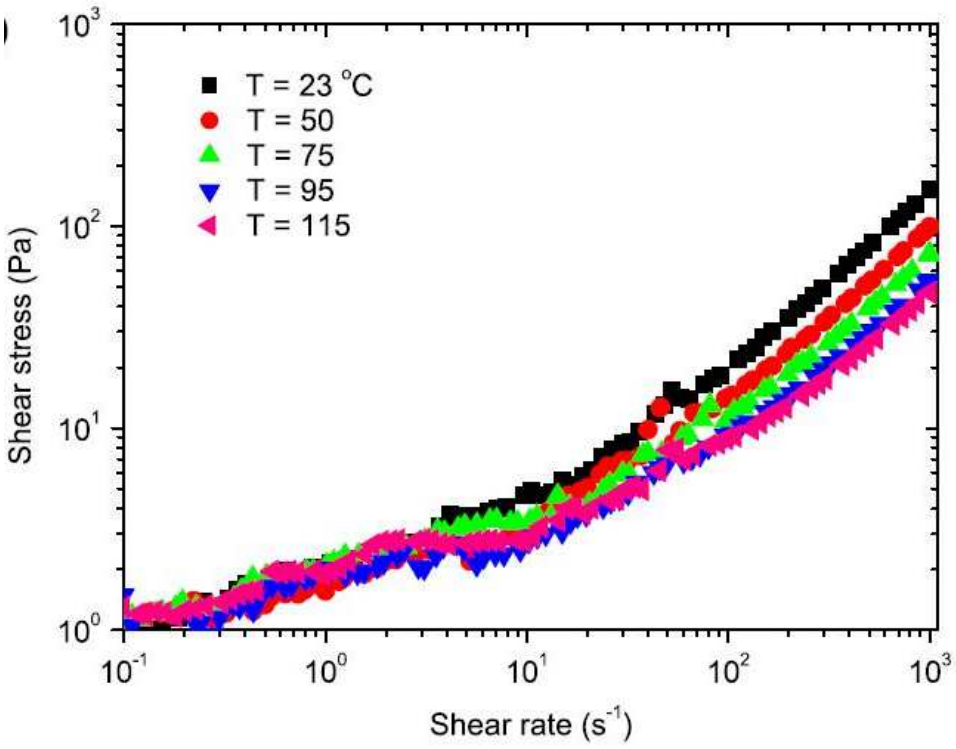

Figure 20: Flow curve of shear stress versus shear rate under zero electric field for the 10 vol%. PANi-CT/ silicone oil ER suspension at different temperatures [50].

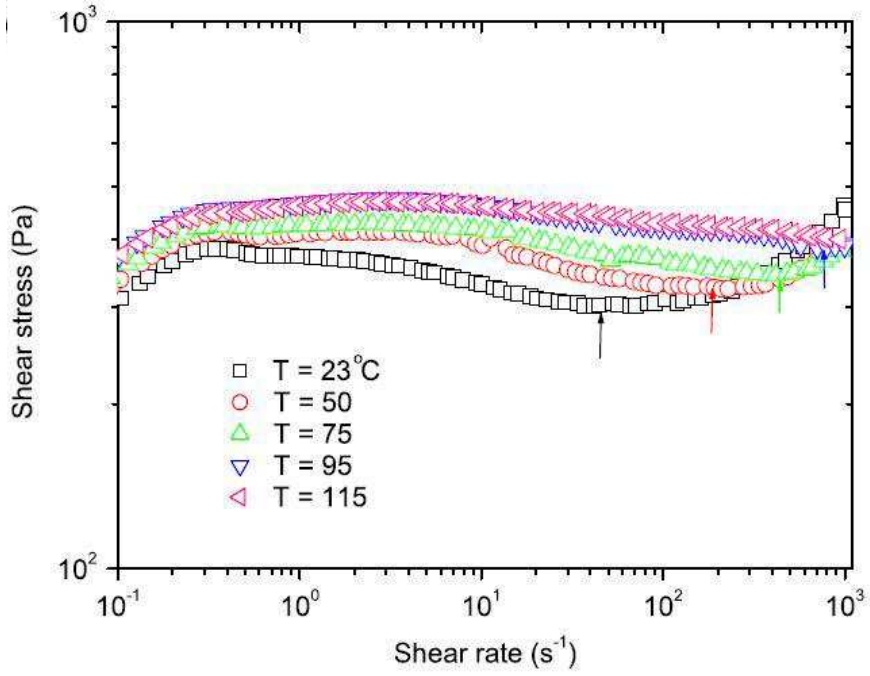

Figure 21: Flow curve of shear stress versus shear rate under electric field (E= 3kV/mm) for the 10 vol. % PANi-CT/Silicone oil suspension at different temperatures [50].

2.3.5 EFFECT OF PARTICLE DIELECTRIC PROPERTIES

Particles dielectric properties highly influence the ER effect, thus the dielectric measurements of ER fluids are frequently used for investigating the efficiency and extent of the ER effect. Moreover, the dielectric constant of the ER fluid changes with the changes in applied electric field strength. It was found that the dielectric constant increases with the increase in electric field strength and saturates or levels off at higher electric field strength when the particle volume concentration is below 10%, whereas the dielectric constant tends to decrease with electric field strength if the particle volume concentration exceeds 46% [38].

2.3.6 EFFECT OF THE CHOICE OF LIQUID MEDIUM

The different liquid medium (dispersion medium) gives a significant difference in the observed ER effect. It also alters the particle sedimentation owing to the different density of the liquid medium and it influences the viscosity of whole suspension at zero electric field. It is found that, the same particulate material displays a different ER effect in in different liquid medium [38].

3 APPLICATIONS OF ER FLUIDS

Unique feature of ER fluids as their mechanical strength can be instantly and reversibly changed by the application of electric filed (thanks to the instant change in physical state i.e., from liquid to solid) has made them the ideal candidate in the fabrication of electro-mechanical transducers. Some of the important applications of ER fluids are discussed below [51].

3.1 ER VALVES AND THEIR AUTOMOTIVE APPLICATIONS

Over the last few years, the possible application of electrorheological (ER) and magnetorheological (MR) fluids in the development and fabrication of controllable dampers has attracted substantial inquisitiveness, particularly in automobile suspension systems [52].

Robust, constantly adjustable servo valves are normally used in hydraulic applications with precise accuracy. In recent years ER valves have been used in servo drives, dampers and in brakes. In the conventional hydraulic valves, the flow rate is controlled or altered by spool movements. But in an ER valve the flow rate is directly controlled by means of changing the apparent viscosity of the ER fluid by applying sufficient external electric field, which is more attractive because in ER valves the moving parts such as the spool are necessary as in servo valves [53].

3.1.1 ER FLUID CONTROLLED DAMPERS

In order to improve the ride comfort and stability semi-active suspension systems comprising an adjustable damper are increasingly installed in automobiles. In conventional semi-active dampers, the hampering is adjusted by means of an electromagnetic valve. In recent years, adjustable dampers based on smart fluids (electro or magnetorheological fluids) have been introduced [54].

For example, a bypass damper is shown in Fig 22, it consists of a hydraulic cylinder, which is divided into two working chambers by a piston. The bypass consists of two concentric tubular concentric electrodes and an opening though which the ER fluid flows, is fitted to the side of the hydraulic cylinder [56].

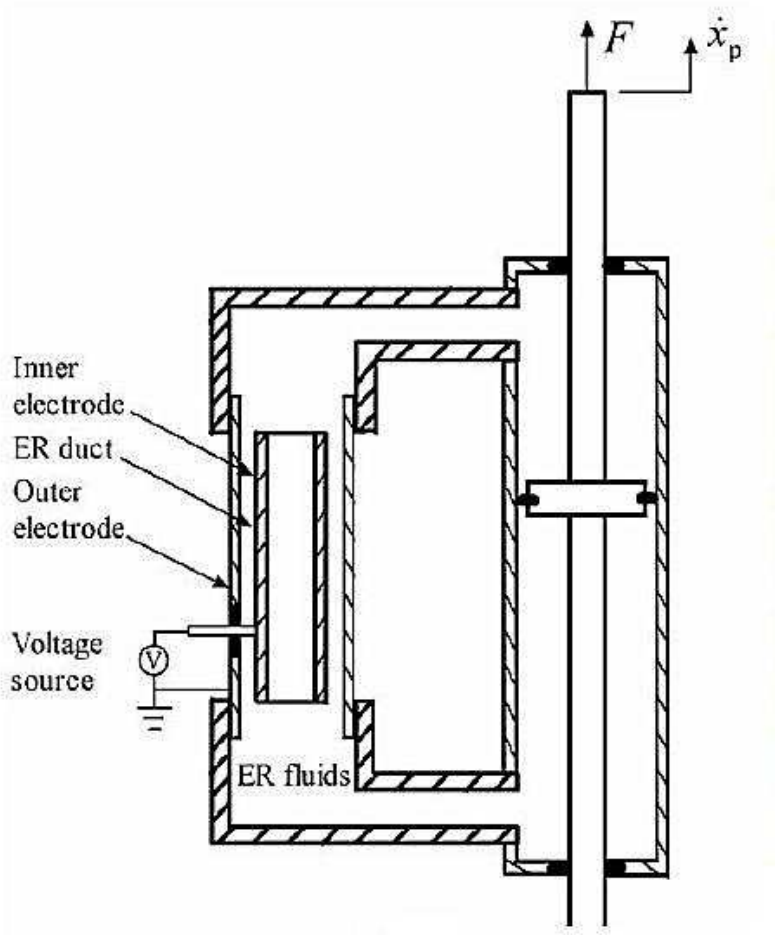

Figure 22: Schematic configuration of the bypass type ER damper [55]

The inner electrode is connected to the positive terminal of voltage supply unit, while the outer electrode is connected to the negative voltage terminal. In the absence of electric field, the damping force is delivered only by means of the inherent fluid resistance.

However, an additional damping force is created when sufficient amount of electric voltage is applied to the system. This is due to the surge in yield stress of the ER fluid.

Moreover the efficiency of the ER damper can be continuously tweaked by changing the voltage supply. Figure 23, shows the measured damping force with respect to the piston velocity at various Voltages. It is obtained by calculating the maximum damping force at each velocity. Such a plot is frequently employed to evaluate the level of damping performance in damper manufacturing industry [55].

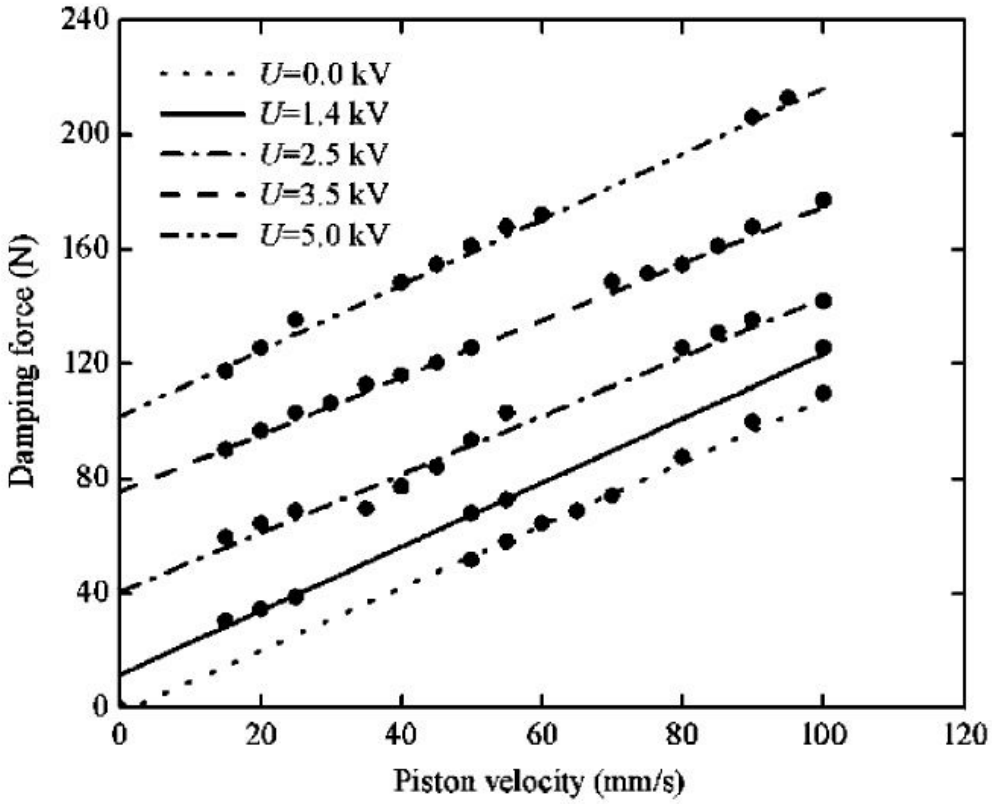

Figure 23: Damping force versus piston velocity at various voltages [56]

3.1.2 HYDRODYNAMIC CLUTCH

Clutches and brakes are usually employed when machine needs to be accelerated or stopped respectively [56].

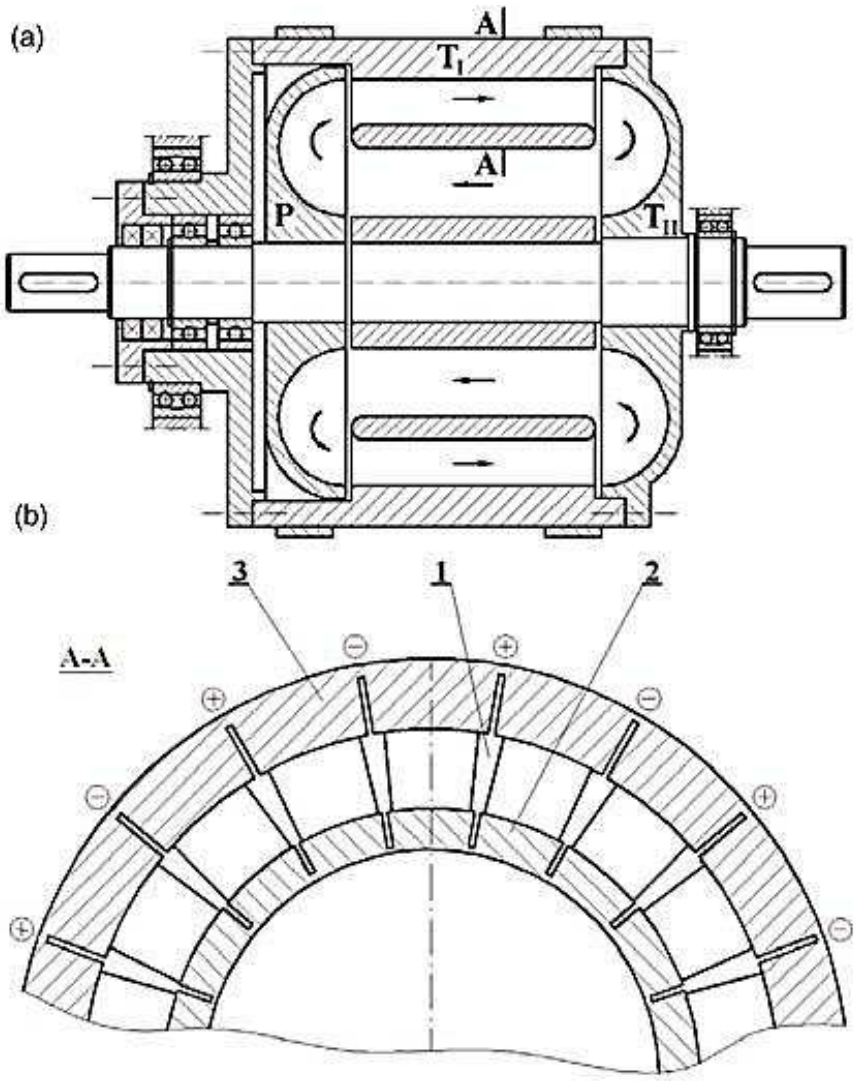

Figure 24: Arrangement of a hydrodynamic clutch with ER/MR fluid: P—pump with mixed through-flow, T_I—first section of turbine with axial flow, T_{II}—second section of turbine with mixed through-flow, 1—wedge shape blade, 2—inside housing wall, 3—outside housing wall [57]

The main parts of a hydrodynamic clutch are a pump and a turbine mounted in a housing filled with a working fluid. When the pump rotates, torque is transmitted to the turbine by fluid circulation in the channels. By using ER fluid inside the turbine housing as the working fluid, the torque transmission can be controlled by varying the electric field strength supplied to ER fluid. However, use of MR suspensions in such system is much more effective over the ER fluids [57].

3.1.3 PADLESS ULTRAPRECISION POLISHING

Using the ER fluid a new type of polishing method to achieve mirror surface finish is developed. A polishing slurry composed of ER fluid and an abrasive is used to achieve the desired polished surface finish [31, 58].

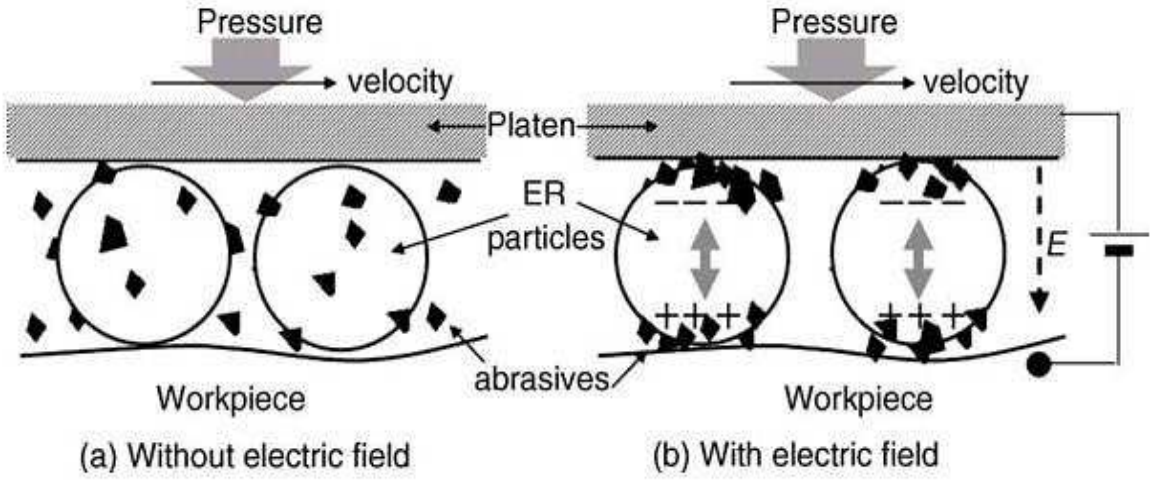

Figure 25: The principle of ER fluid assisted material removal [58]

At the interface between the work piece and the moving platen the ER fluid is placed, the friction force can be adjusted according to the desired surface finish by varying the applied voltage, this type of microscopic precision polishing methods can be employed in the fabrication of silicon wafer chip [58]

3.1.4 REHABILITATION DEVICES

Robotics and Mechatronics Laboratory have developed a latest active knee rehabilitation device using the ER fluids. As shown in the Fig. 26, It's a device consists of a number of concentric cylinders tightly fit one inside the other leaving only a small gap in between them, and the gap between the cylinders is filled with ER fluid, when computer-controlled electric voltage is applied to the cylinders, the liquid inside the gap turns solid in less than a millisecond, creating resistance on a healing joint. The computer chip mounted on the device offers a real-time modification of the resistance for posture retraining and the amount of resistance can also be modified by the patient by altering the amount of applied electric voltage [59].

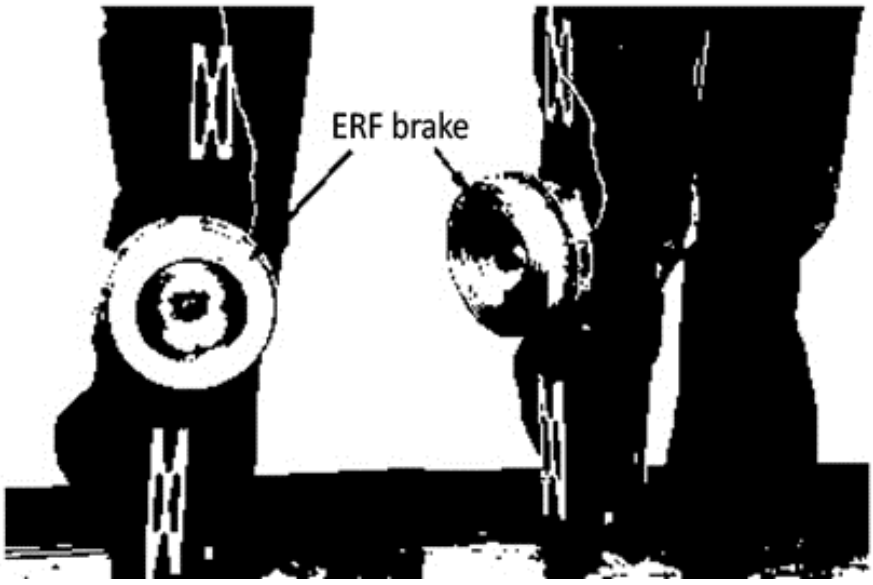

Figure 26: AKROD Electro-Rheological Fluid knee Joint [59].

II. ANALYSIS

4 AIM OF WORK

The aim of this master thesis is

- Preparation of PPy samples with different amount of Ag content.
- Characterization of prepared PPy and PPy-Ag composite particles.
- Determination of rheological and dielectric properties.
- Evaluation of obtained results.

5 SYNTHESIS OF POLYPYRROLE – SILVER COMPOSTIES

PPy-Ag composite particles of various amount silver content as shown in Table 1, is prepared using vacuum distilled Pyrrole (Py, 98%) and ammonium peroxydisulfate (APS, 98%, $(NH_4)_2S_2O_8$), or with the mixture of various molar solutions of APS and silver nitrate (99%, $AgNO_3$). Distilled water is used as solvent medium to make all the molar solutions. All the reagents used were purchased from Sigma Aldrich Chemicals.

The molar concentrations of oxidative reagents (APS and $AgNO_3$) were chosen in such a way that each mole of the reagent oxidise half mole of Py. For example, S3 is prepared using the oxidative reagents in the ratio of 1:2 because APS is a two-electron oxidant on the other hand $AgNO_3$ is a one-electron oxidant.

Table 1: Composition of reaction mixtures

Sample	**APS (Mole)**	**$AgNO_3$(Mole)**	**Reaction time (Hr)**
S1	0.2	0	4.0
S2	0.15	0.1	4.5
S3	0.1	0.2	6.0
S4	0.05	0.3	46.0
S5	0	0.4	46.0

To prepare PPy with various amount of Ag, the oxidation polymerization reactions were carried out in a manner as described below.

0.2 M of Py was taken in a three necked flask as shown in Fig 28. The reagents (APS and $AgNO_3$) of various molar concentrations as mentioned in the Table 1 were added drop by drop through the sides of the flask.

The whole mixture was constantly stirred using a magnetic stirrer and the temperature of the reaction mixture was frequently monitored (Fig 27). The colour of the mixture turns from clear liquid to dark green yellowish black which is a clear indication that the oxidation occurred.

When the reaction was over the content of the flask was filtered and washed twice using distilled water and ethanol and then it was vacuum dried at 60°C for 6 hours. Later the formed PPy particles were finely grounded and stored in a moisture proof container for later evaluation.

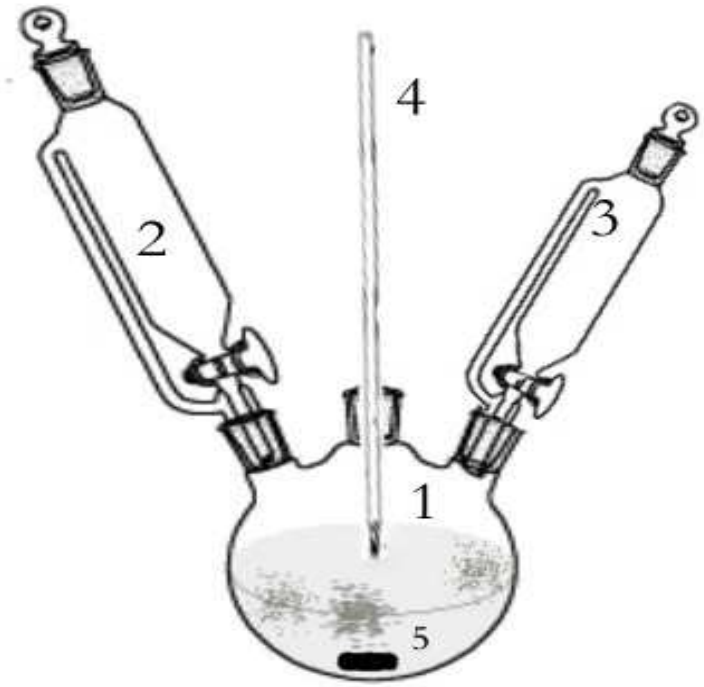

Figure 27: *Apparatus used for the preparation of PPy particles*

1) Reaction flask (2) & (3) Pressure equalized addition funnels (4) Thermometer (5) Stirrer

Since, the oxidative polymerization reaction of Py with the APS and APS/$AgNO_3$ is an exothermic reaction the temperature of the reactive mixture is a virtuous indicator for the evaluation of reaction time (Fig 28).

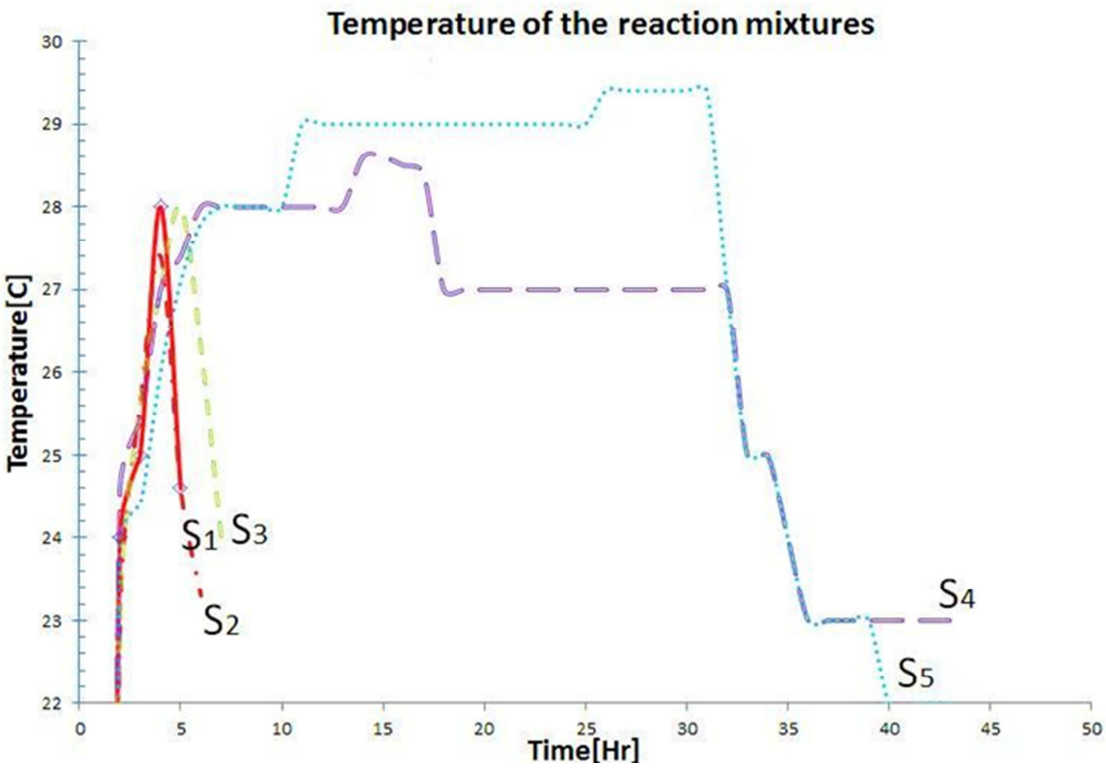

Figure 28 Temperature of the reaction mixture (PPy-APS/$AgNO_3$) over time

In order to adjust prepared particles conductivity to the optimal range of 10^{-5} to 10^{-8} $S.cm^{-1}$, the prepared samples were depronataed by treating the samples with 300 ml of 1 M ammonium hydroxide and dried as mentioned previously. The sample S1 was prepared twice and one of which was depronated twice by performing the same deprona-tion method as described above.

5.1 CHARACTERIZATION METHODS

5.1.1 SEM, XRD, TGA AND FTIR ANALYSIS

To observe the morphologies of PPy and PPy-Ag composite particles a scanning electron microscope (SEM, VEGA II LMU, Tescan Ltd., Czech Republic), with an operating voltage of 10 kV was adopted. Furthermore, the presence of Ag in the prepared samples was confirmed through the X-ray diffraction (XRD) pattern collected using the X'pert PRO diffractometer (Phillips, The Netherlands) employing Cu $K\alpha_1$ radiation (λ = 0.154 Å) and a scanning rate of 4° min^{-1} for recording the data in the wide range of 2θ = 5 - 95°.

To find the amount of Ag present in each sample thermogravimetric analysis (TGA, TA Instruments Q500, USA) under normal atmospheric conditions at a heating rate of 10°C min^{-1} was chosen. Fourier transform spectroscope (FTIR, Thermo Scientific, USA) was used to obtain IR spectra in the range of 680-4000 cm^{-1} at 64 scans per spectrum at 2 cm^{-1} resolution attenuated total reflectance (ATR) technique with Germanium crystal.

And the density of the synthesized PPy and PPy-Ag composites was determined using a Pycnometer at 25 °C.

5.1.2 CONDUCTIVITY MEASUREMENTS

The conductivity of the PPy-Ag composite particles was measured at room temperature using a multimeter (Keithley Instruments Inc., USA) by the four-point van der Pauw method on the pelletized samples (13 mm in diameter and 1-1.3 mm thickness), the pellets were made using a manual hydraulic press using Keithley 6517A and 7001 at 600 MPa.

5.1.3 ELECTRORHEOLOGICAL MEASUREMENTS

The finely grounded PPy / PPy-Ag composite particles were dispersed in silicone oil (Lukosiol M200, Chemical works Kolín, Czech Republic: ηc = 200 mPa.s, ρ = 0.97 $g.cm^{-3}$) to prepare ER fluids of 5 and 10 vol. %. At first, suspensions were mechanically stirred using a clean glass rod and then subjected to sonification for 1 min before each experiment.

Rheological properties of the ER fluids were measured using a rotational rheometer Bohlin Gemini (Malvern Instruments, UK) with parallel plates of 40 mm in diameter and a gap of 0.5 mm between them. A direct current (DC) voltage was generated by a TREK DC high-voltage source (TREK 668B, USA).

At first the DC voltage was applied for 60 seconds to facilitate the generation of equilibrium chain-like structures in suspension prior to shear measurements. The steady-flow measurements were performed in the shear rate range of 0.1-300 s^{-1} under controlled shear rate (CSR) mode.

The oscillatory tests were carried out through dynamic strain sweeps and frequency sweeps. The strain sweeps were performed in the applied strain range of 10^{-4} to 10^{-2} at a fixed angular frequency of 6.28 rad s^{-1} under an electric field in order to get the position of the linear viscoelastic region (LVR). Afterwards, the viscoelastic moduli were obtained from the frequency sweep tests (0.5 to 100 rad s^{-1}) at fixed strain amplitude in the LVR. All the oscillatory measurements were performed in CSR mode.

In the both modes before each measurement at new electric field strength, the formed structures within the suspension was destroyed by shearing at a shear rate of 20 s^{-1} for 120 s. The experiments were carried out at 25 °C.

5.1.4 DIELECTRIC MEASUREMENTS

Frequency dependences (in range of 40^{-5} x 10^{6} Hz) of dielectric constant ε' and dielectric loss factor ε" of 5 vol. % samples of the ER fluids were measured using an impedance analyser (Agilent 4524, Japan) at 25°C.

6 RESULTS AND DISCUSSIONS

6.1 MORPHOLOGY OF PPy & PPy-Ag COMPOSITE PARTICLES

Scanning electron microscopy (SEM) was performed in order to investigate the dimensions and the morphology of PPy and PPy-Ag composite particles. The scanning electron micrographs are presented in Figure 29 to 33.

As can be seen, the particles have globular shape and it is also evident that the sizes of the resulting particles tend to increase a bit as the concentration of $AgNO_3$ in the reaction mixture increases. The polypyrrole particles are observed to have a distribution of dimensions between 0.1–0.3 µm. However, the shape of the particles totally changed into something broccoli-like agglomerates when only $AgNO_3$ is employed as an oxidizing agent (Fig 33). The faint white spots in the Figs 30-33 can be attributed to the Ag particles.

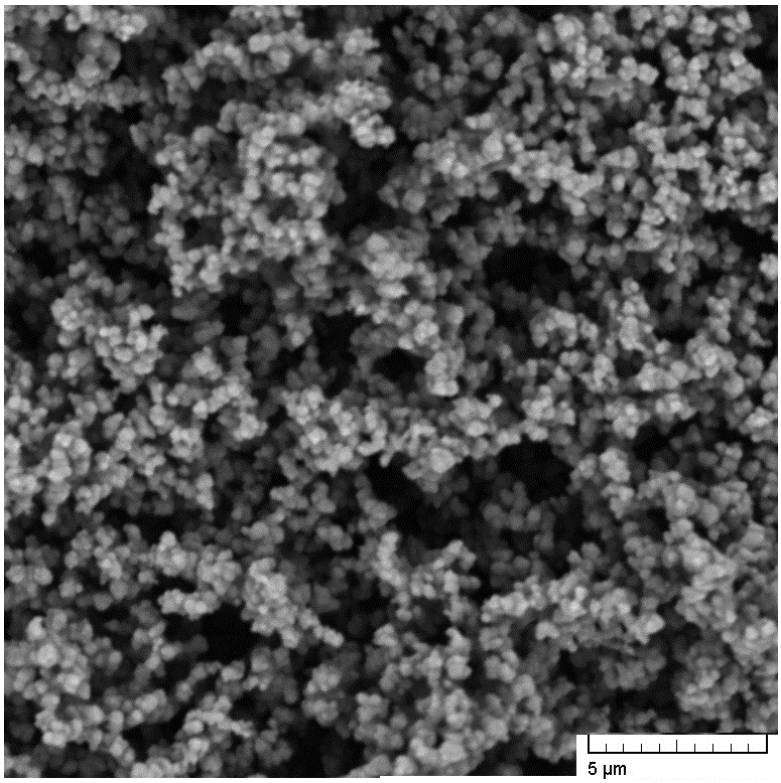

Figure 29: SEM micrograph of Sample S1

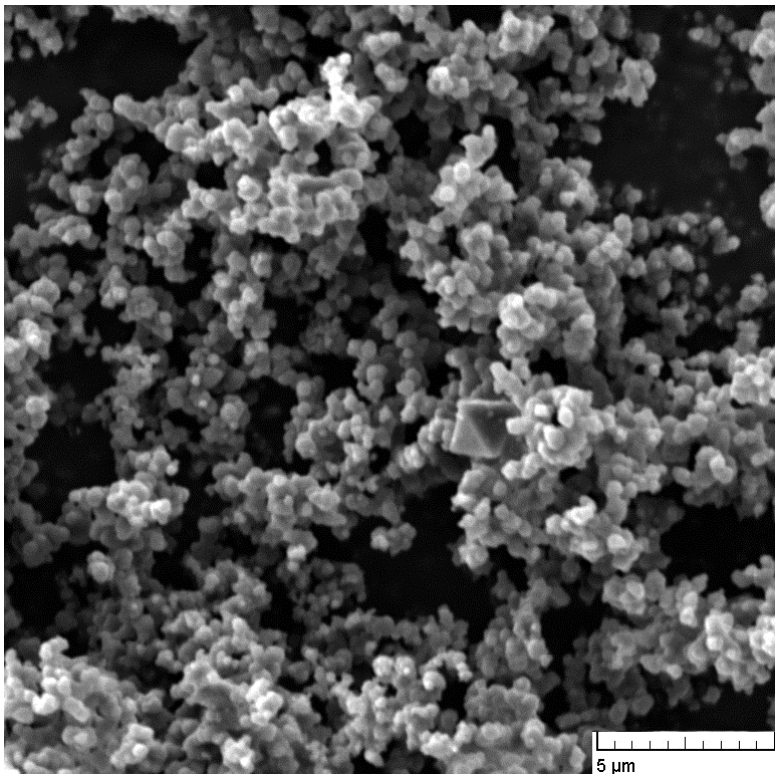

Figure 30: SEM micrograph of Sample S2

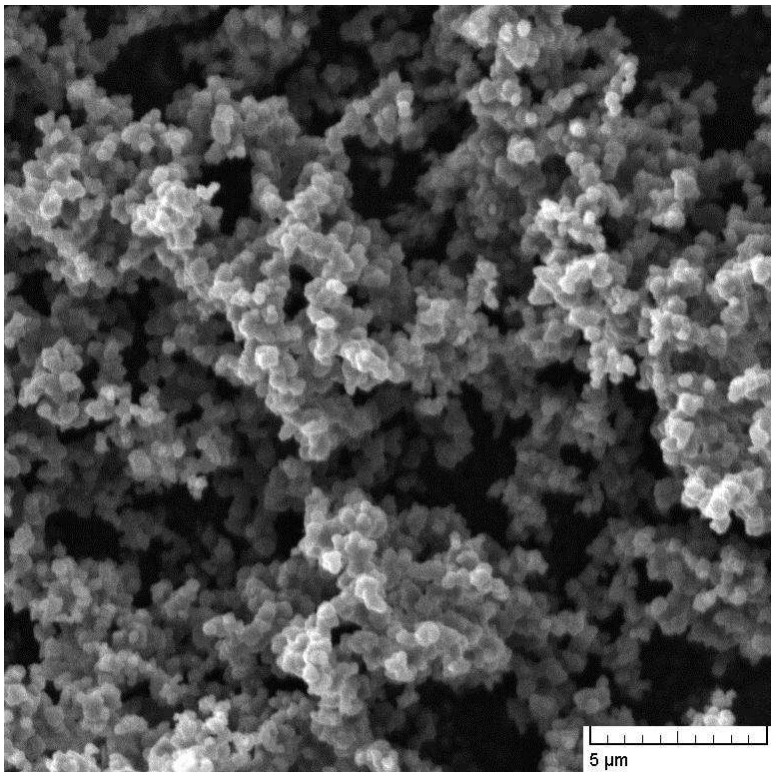

Figure 31: SEM micrograph of Sample S3

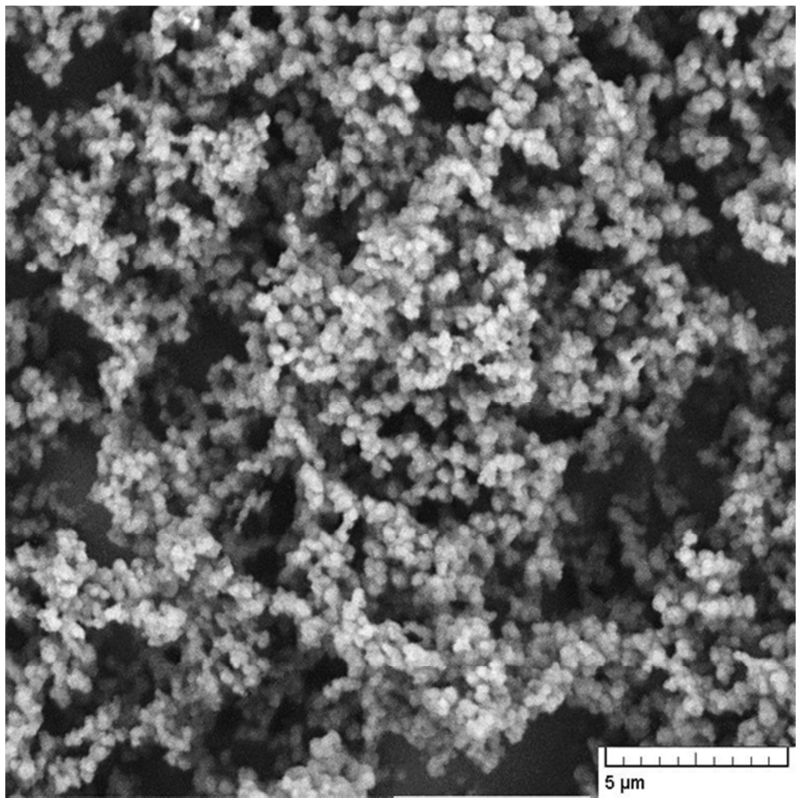

Figure 32: SEM micrograph of Sample S4

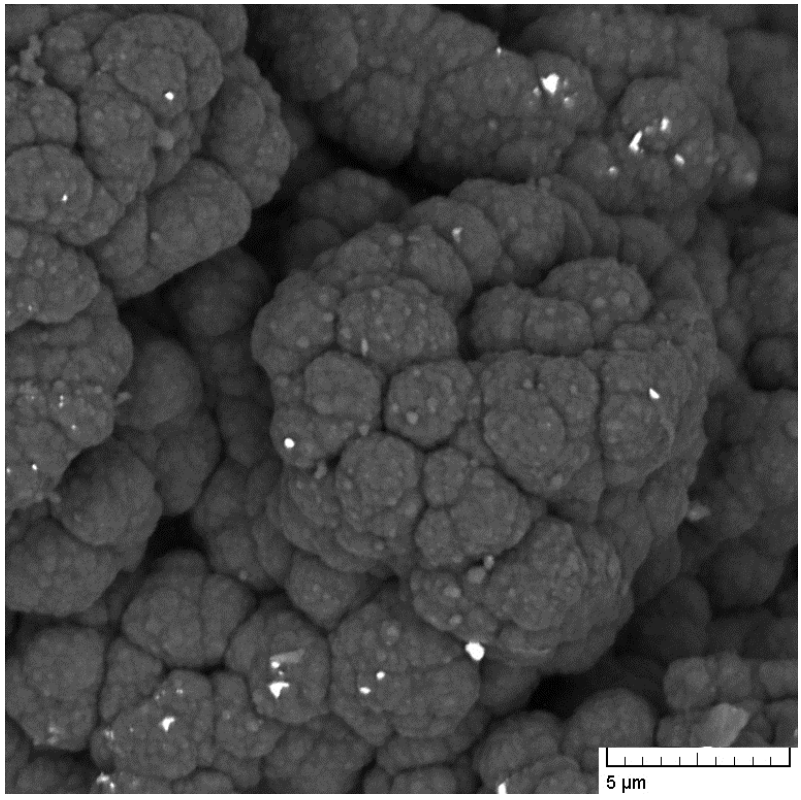

Figure 33: SEM micrograph of Sample S5

6.2 FTIR STUDIES ON THE SAMPLES

FTIR analysis was carried out to identify PPy and any changes in its chemical structure because of the different concentrations of oxidants used.

For all the samples, the characteristic peaks are observed at 823 cm^{-1}(=C – H out of ring plane vibrations), 914 cm^{-1} (C – C out of phase), 1043 cm^{-1}(=C – H in plane vibrations), 1196 cm^{-1} (PPy ring bending), 1290 cm^{-1} (C – C bond), 1475 cm^{-1} (PPy ring vibrations), 1558 cm^{-1} (C = C bond), 1684 cm^{-1} (C=N bond), 3108 cm^{-1} (N – H stretching vibrations) which confirms the formation of PPy.

However some small shift toward lower wave numbers due to the addition of Ag on certain peaks can be observed, Fig 34.

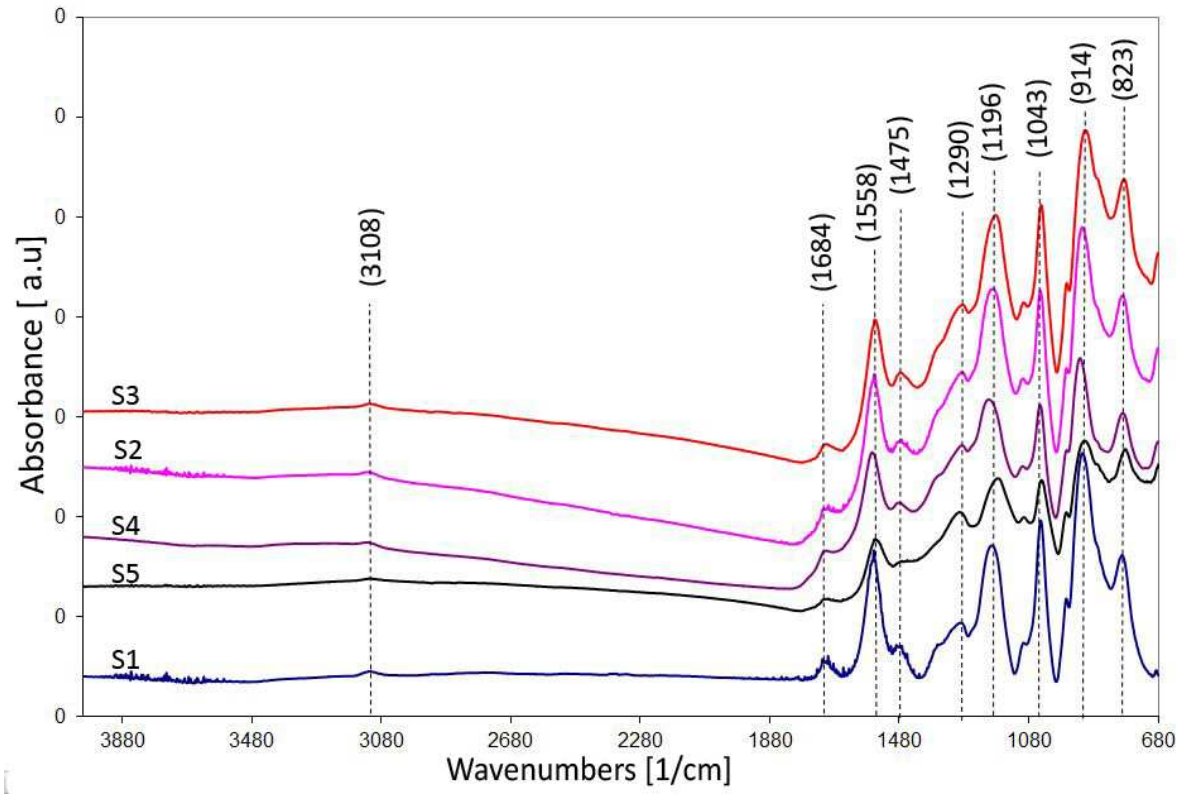

Figure 34: FTIR spectra of prepared samples

6.3 CHARACTERIZATION OF PPy and PPy-Ag PARTICLES

Table 2, shows the results obtained from four-point van der Pauw method, the TGA measurements on the samples of PPy/PPy-Ag composite particles and their densities. The results are explained in detail in the following sections.

Table 2: The molar concentrations of oxidants APS and $Ag.NO_3$ (C) used for the synthesis of particles employed in ER fluids and their density (ρ), amount of Ag (w_{Ag}) and conductivity (σ_{DC}).

Sample	C_{APS} **[mol.l^{-1}]**	$C_{Ag.NO3}$ **[mol.l^{-1}]**	ρ **[g.cm^{-3}]**	W_{Ag} **[Mass %]**	σ_{DC} **[x10^{-6} S.cm^{-1}]**
$S1_{2x}$	0.2	0	1.153	0.0	0.29
S1	0.2	0	1.153	0.0	1.60
S2	0.15	0.1	1.628	44.2	9.21
S3	0.1	0.2	2.632	63.5	10.72
S4	0.05	0.3	2.496	72.3	252
S5	0	0.4	4.462	78.4	

***** $S1_{2x}$ (Twice deprotonated)

It is worth stating that 'when the content of Ag was increased to 0.4 mol.l^{-1}, the resulting PPy-Ag composite particles were denser and consisted of distinct particles (like beach sands) and it was not possible to make stable pellets in order to perform the conductivity measurements as per van der Pauw method'.

As expected, when the content of Ag was increased from 0.1 to 0.4 mol.l^{-1}, the density of the resultant PPy-Ag composite particles was also increased. Furthermore, the presence of Ag and its weight percentage in each sample were confirmed by XRD analysis and TGA respectively.

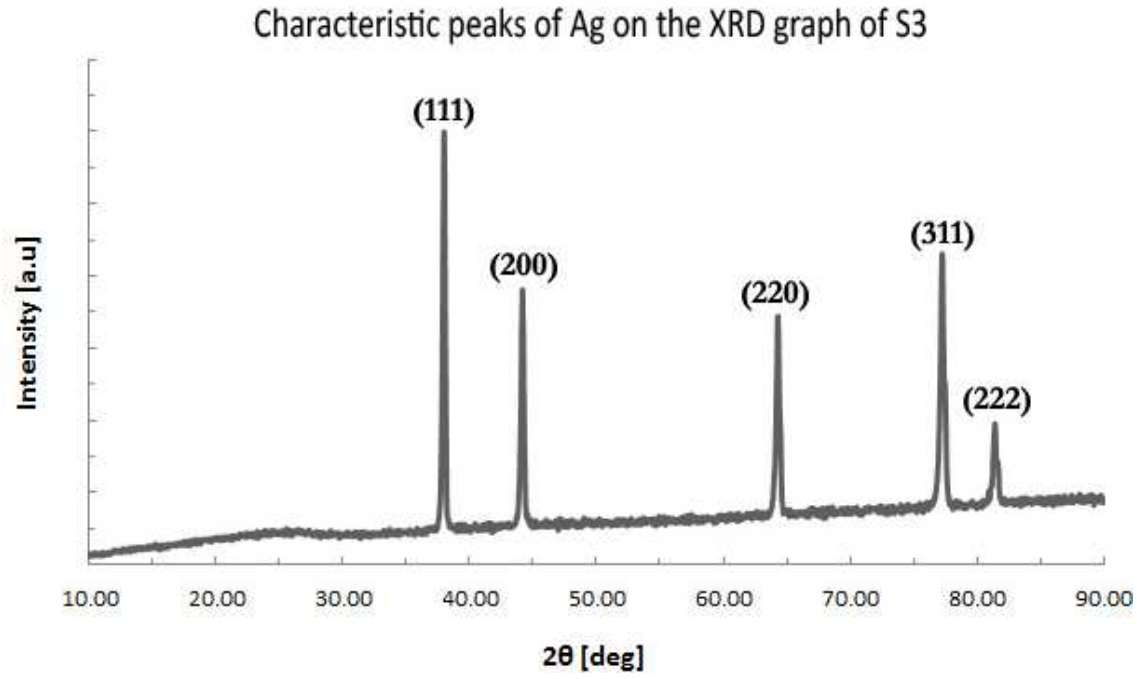

Figure 35: XRD pattern of S3 confirms the presence of Ag

As shown in Fig 35, the peaks obtained can be indexed to the cubic structure of Ag with the lattice constant of 4.0862 Å and a small amorphous halo due to the presence of PPy in the sample is also evident from the XRD.

Thermograms from TGA experiments of the samples are shown in Fig. 36, through which it is possible to calculate the amount of Ag present in each samples. As the amount of Ag via molar concentration of $AgNO_3$ (from 0.1 to 0.4 mol.l^{-1}) increased, the amount of Ag in the PPy-Ag composite also increased from (44.2 to 78.4 wt. %), consequently which results in the increase in density and conductivity of the samples as can be seen in Table 2.

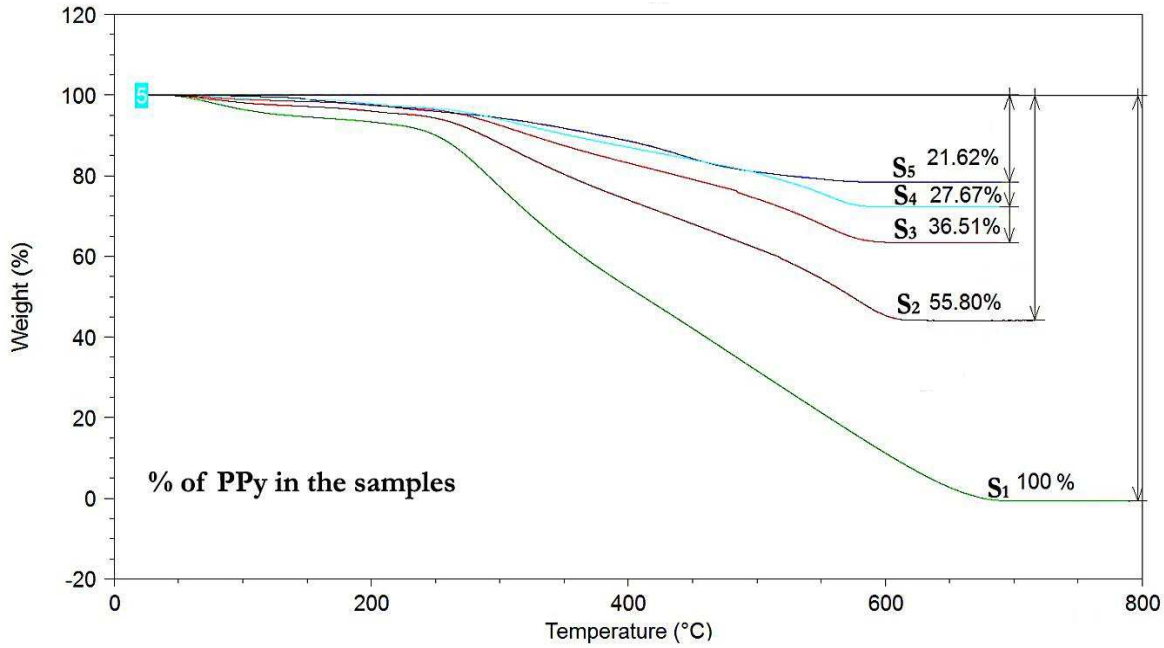

Figure 36: Thermograms of prepared samples indicating the amount of PPy present in each of them

6.4 Electrorheological measurements

Figures 37-40, show the flow curves for the prepared ER fluids samples S1, S2, S3 and $S1_{2x}$ of PPy and PPy-Ag composite particles, under different electric fields. Under the absence of an electric filed all samples exhibit almost a Newtonian behavior i.e. The shear stress increases linearly with shear rate. Whereas in the presence of an electric field, a dramatic increase in the shear stress is observed and all the samples exhibit a distinct yield stress, demonstrating a shear thinning behavior.

The increase in yield stress and the shear stress with the increasing electric filed strength is clearly visible from the following graphs and the values of yield stress of the samples are tabulated in Table 3.

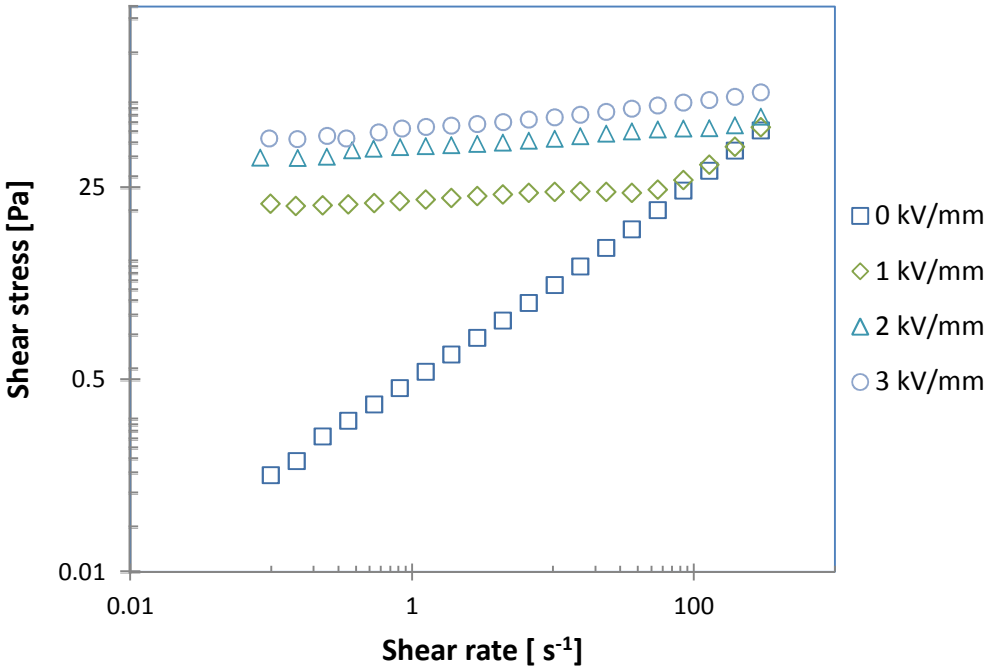

Figure 37 : Dependence of shear stress (τ), on shear rate ($\dot{\gamma}$), for 5 vol. % sample of S1 at various electric field strengths E (kV/mm)

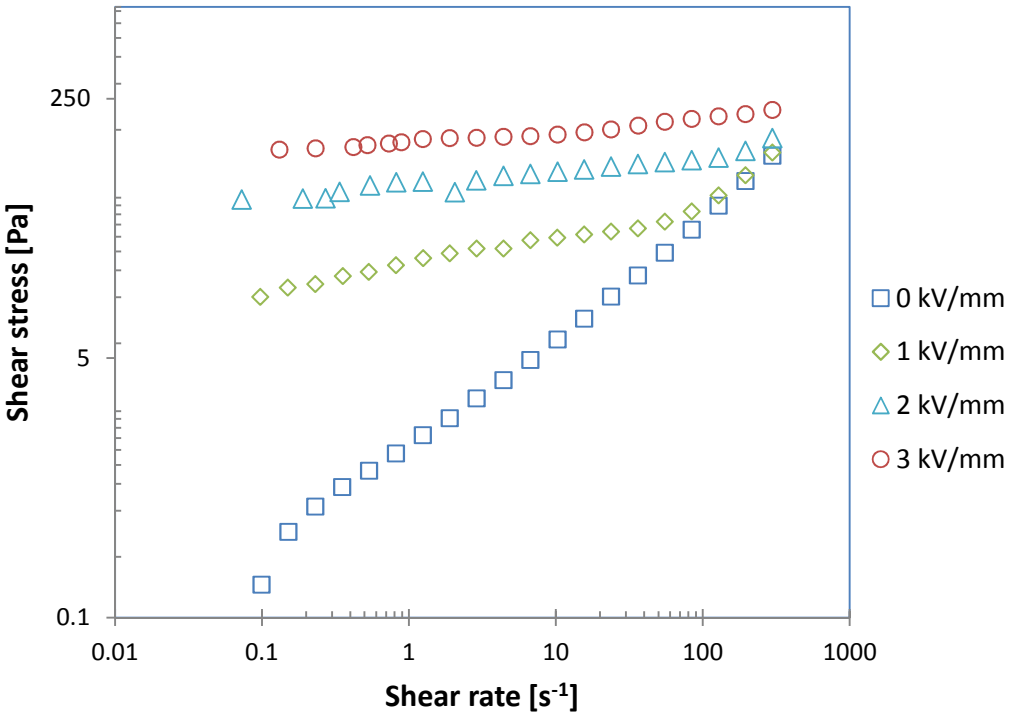

Figure 38: Dependence of shear stress (τ), on shear rate ($\dot{\gamma}$), for 5 vol. % sample of $S1_{2x}$ at various electric field strengths E (kV/mm)

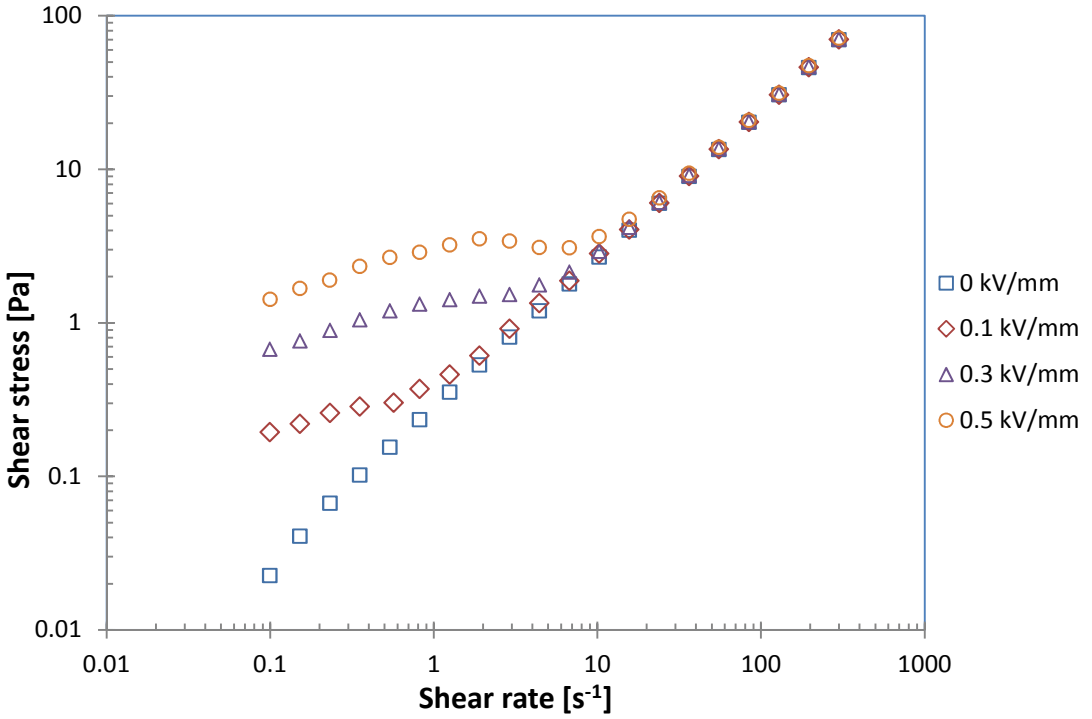

Figure 39 : Dependence of shear stress (τ), on shear rate ($\dot{\gamma}$), for 5 vol. % sample of S2 at various electric field strengths E (kV/mm)

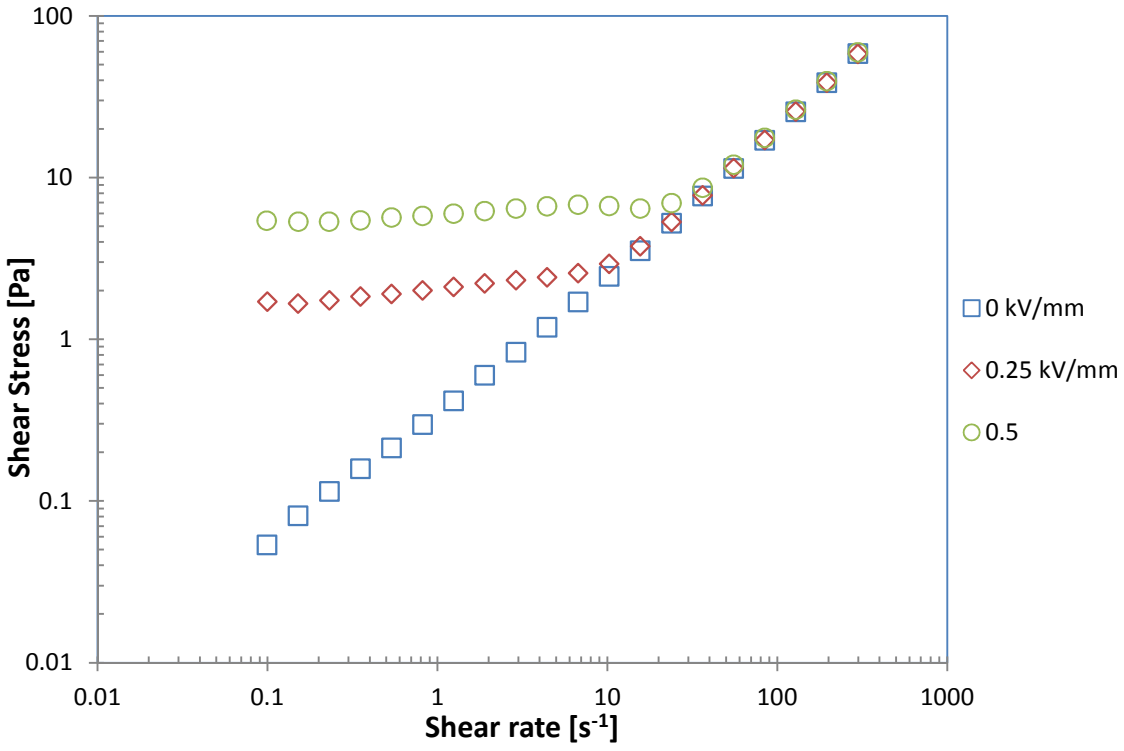

Figure 40: Dependence of shear stress (τ), on shear rate ($\dot{\gamma}$), for 5 vol. % sample of S3 at various electric field strengths E (kV/mm)

As can be seen from the graphs in the presence of an electric field, a dramatic increase in the shear stress is observed and all the samples exhibit a distinct yield stress, demonstrating a shear thinning behavior with increasing shear rate when the hydrodynamic forces start to dominate over the electrostatic forces.

Table 3: Yield stress of prepared samples at $\dot{\gamma} = 0.1\ s^{-1}$ and E= 0.3 kV/mm

Sample	Yield stress [Pa]
S1	5.840
$S1_{2x}$	4.300
S2	1.423
S3	5.411

It is also evident form the above graphs 37-40, that the sample S1 and $S1_{2x}$ show better ER effects under higher applied electric strengths up to 3 kV/mm. Whereas the samples S2 and S3 failed to show ER activity above 0.5 kV/mm due to the presence of Ag, which influence the conductivity of the sample. Thereby rendering the samples to short circuit above the applied electric field strength of 0.5 kV/mm.

Moreover it can also be found that the shear stress of the ER fluids of samples S1 and S3 shows a plateau region over a broad range of shear rate comparative to S2. This phenomenon is mainly due to the changes in the microstructures of ER fluids (i.e., rearrangements and destruction). The other reason could be the insufficient amount (below critical value) of Ag content comparative to S3, hence it can act as an impurity in the system which accounts for the corresponding lower yield stress in S2.

Figure 41, shows the shear stress dependency on shear rate of the samples S1, S2 and S3 at 0.3 kV/mm. From which it's clear that the sample S1 and S3 exhibit a plateau region over a broad range of shear rate than S2.

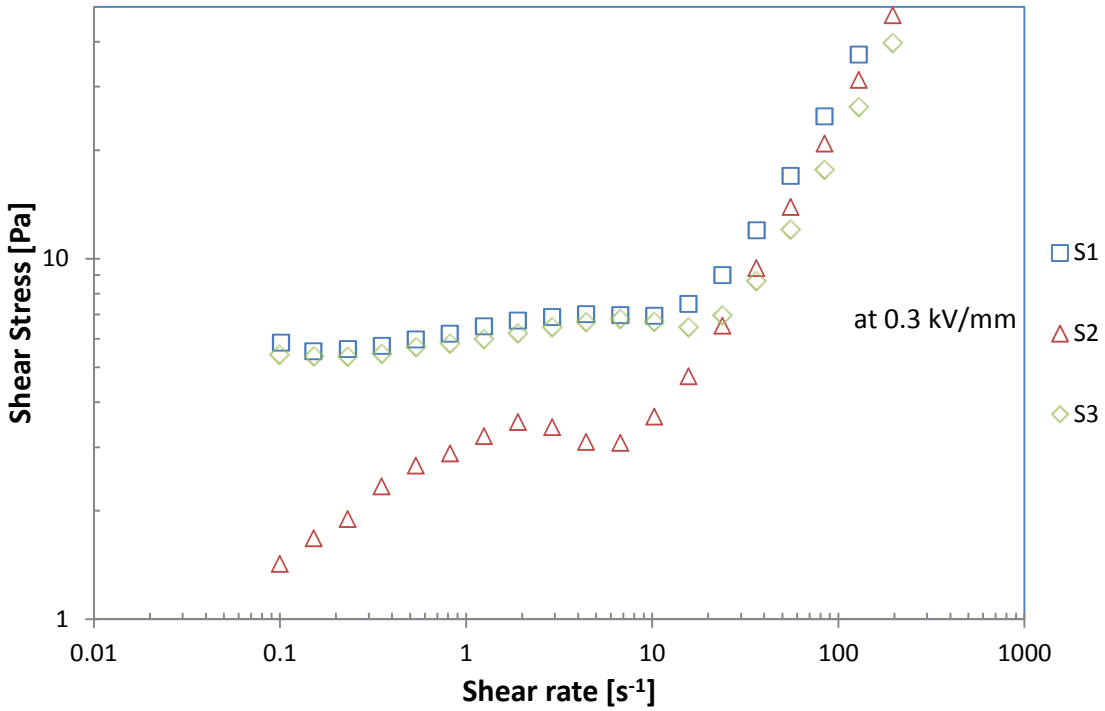

Figure 41: Flow curves of shear stress (τ) as a function of shear rate ($\dot{\gamma}$) for the 5 vol. % ER fluids of S1, S2 and S3 at 0.3 kV/mm

Viscosity as a function of shear rate is shown in Figs. 42-45. Without an applied external electric field viscosity is nearly constant with increasing shear rate and thus exhibits Newtonian behavior.

Under application of electric field viscosity increases significantly with electric field strength and decreases with increasing shear rate. At low shear rates viscosity tends to be the maximum because of the domination of electrostatic forces and the formation of chain-like structures between electrodes which causes viscosity enhancement. At higher shear rates, the viscosity tend to decrease because the hydrodynamic forces become more dominating over the electrostatic ones and the suspensions exhibit pseudoplastic behavior.

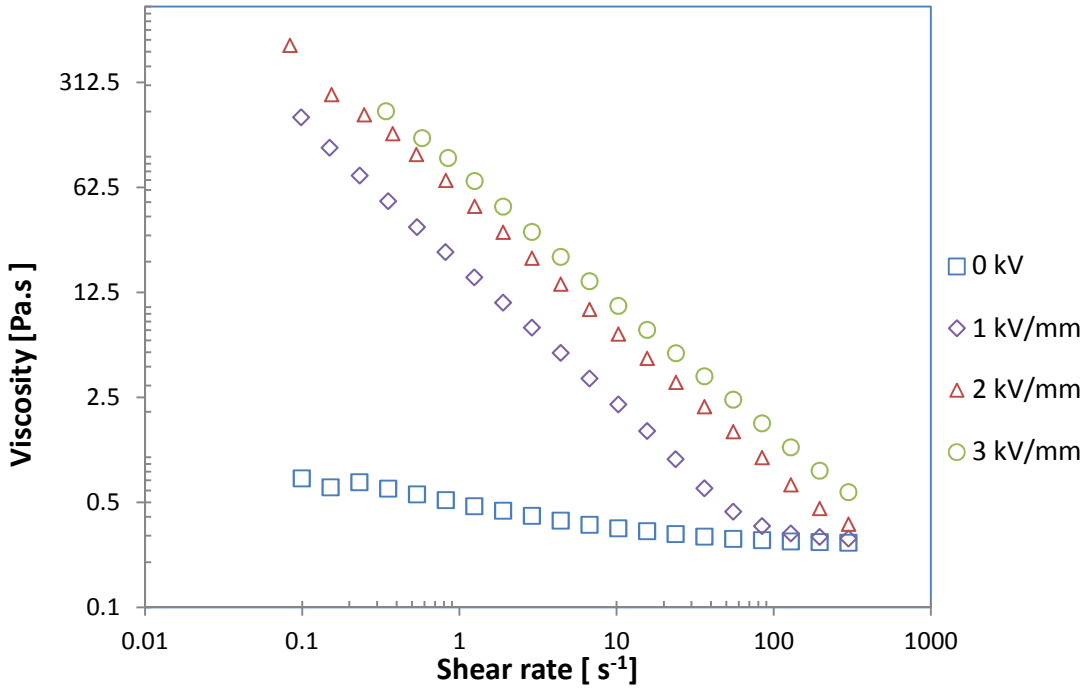

Figure 42: Dependence of shear viscosity (η) on shear rate ($\dot{\gamma}$) for 5 vol. % sample of S1 at various electric field strengths E (kV/mm)

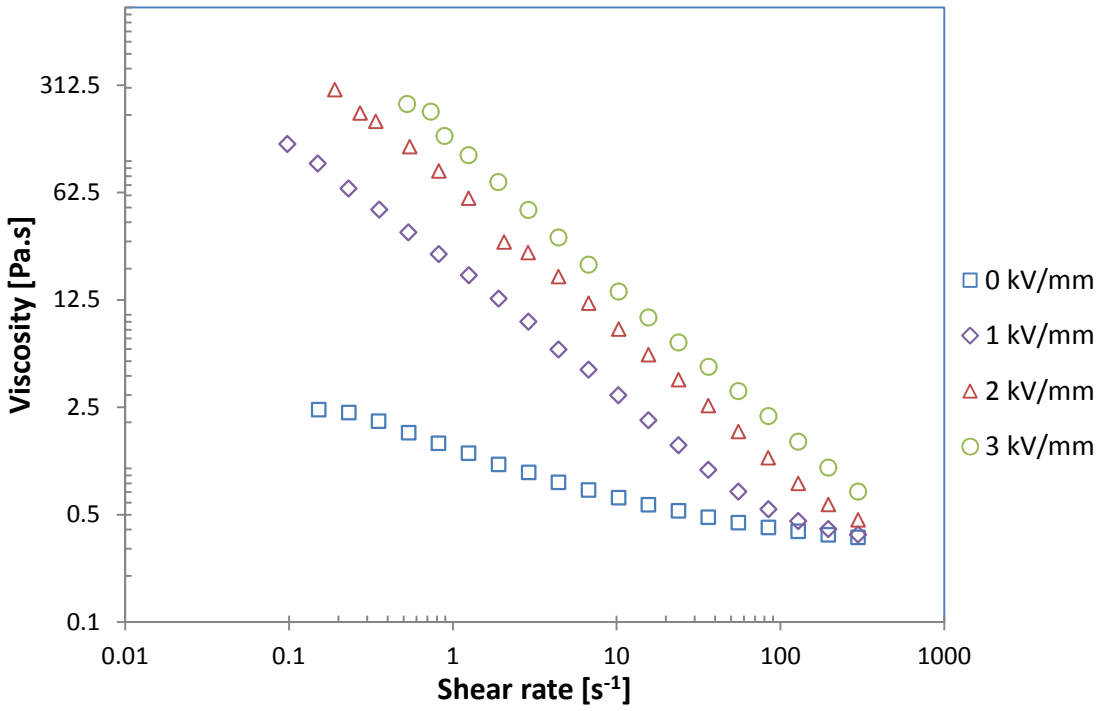

Figure 43: Dependence of shear viscosity (η) on shear rate ($\dot{\gamma}$) for 5 vol. % sample of $S1_{2x}$ at various electric field strengths E (kV/mm)

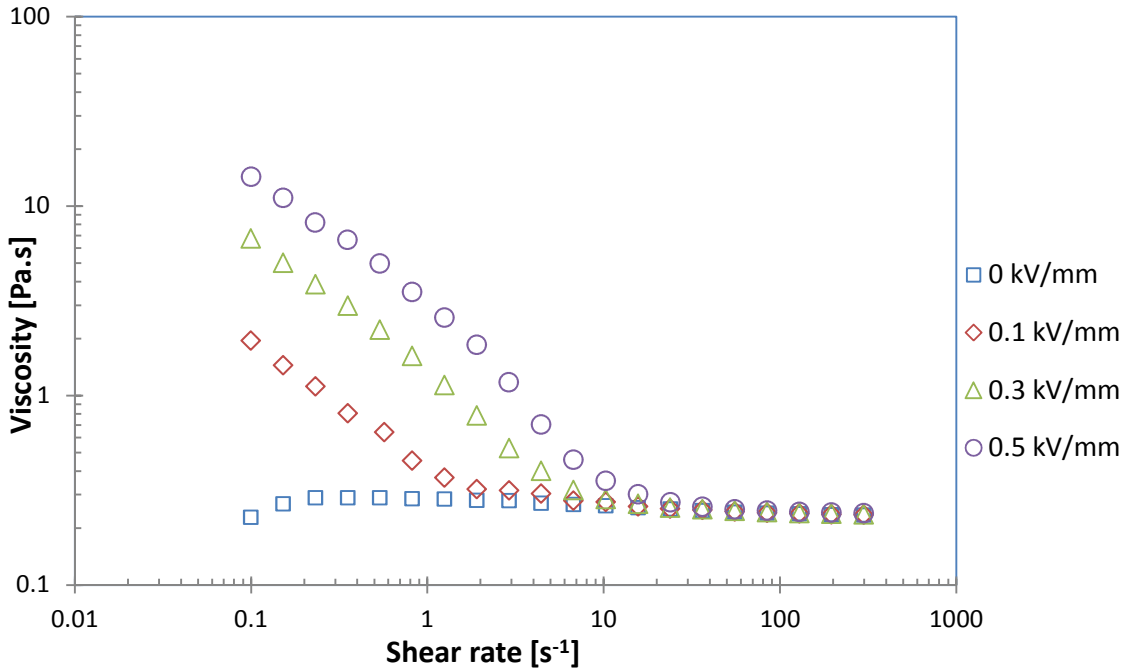

Figure 44 : Dependence of shear viscosity (η) on shear rate ($\dot{\gamma}$) for 5 vol. % sample of S2 at various electric field strengths E (kV/mm)

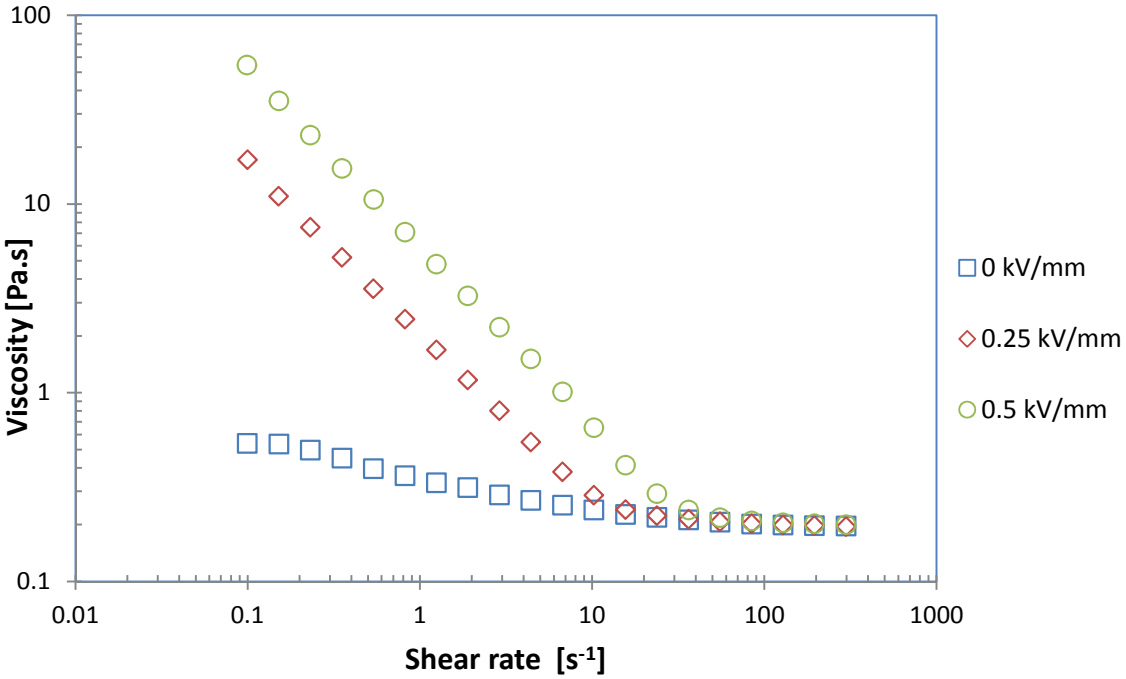

Figure 45: Dependence of shear viscosity (η) on shear rate ($\dot{\gamma}$) for 5 vol. % sample of S3 at various electric field strengths E (kV/mm)

6.4.1 THE EFFECT OF DEPROTONATION

Figure 46 shows the effect of further deprotonation on the sample S1, which is denoted as $S1_{2x}$. It is evident that after double deprotonation the sample exhibit better ER activity due to excess removal of charge carriers along the PPy chain, which enhances the ER activity over the wide range of applied electric field strength with a significant increase in yield stress and in viscosity.

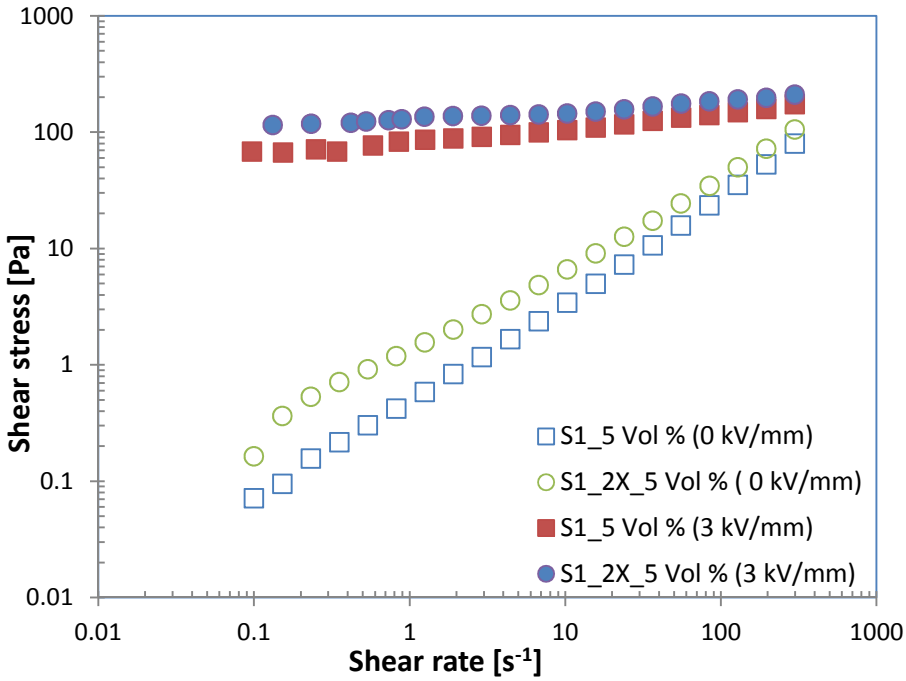

Figure 46: Flow curve (A) and Viscosity curve (B) of 5 vol. % Samples of S1 and $S1_{2X}$ at 0 and 3 kV/mm of applied electric field strength

Furthermore it was possible to make ER suspension of $S1_{2x}$ in Silicone oil with higher particle loading (10 Vol. %) which shows better ER effect than 10 vol. % sample of S1 even under higher electric field strength.

During the rheological experiment the sample S1, which was deprotonated once failed to show ER effect at 3 kV/mm. On the other hand $S1_{2x}$ shows a distinct ER effect with a pronounced increase in yield stress and viscosity at 3 kV/mm, which is evident from the graphs below in Fig 47.

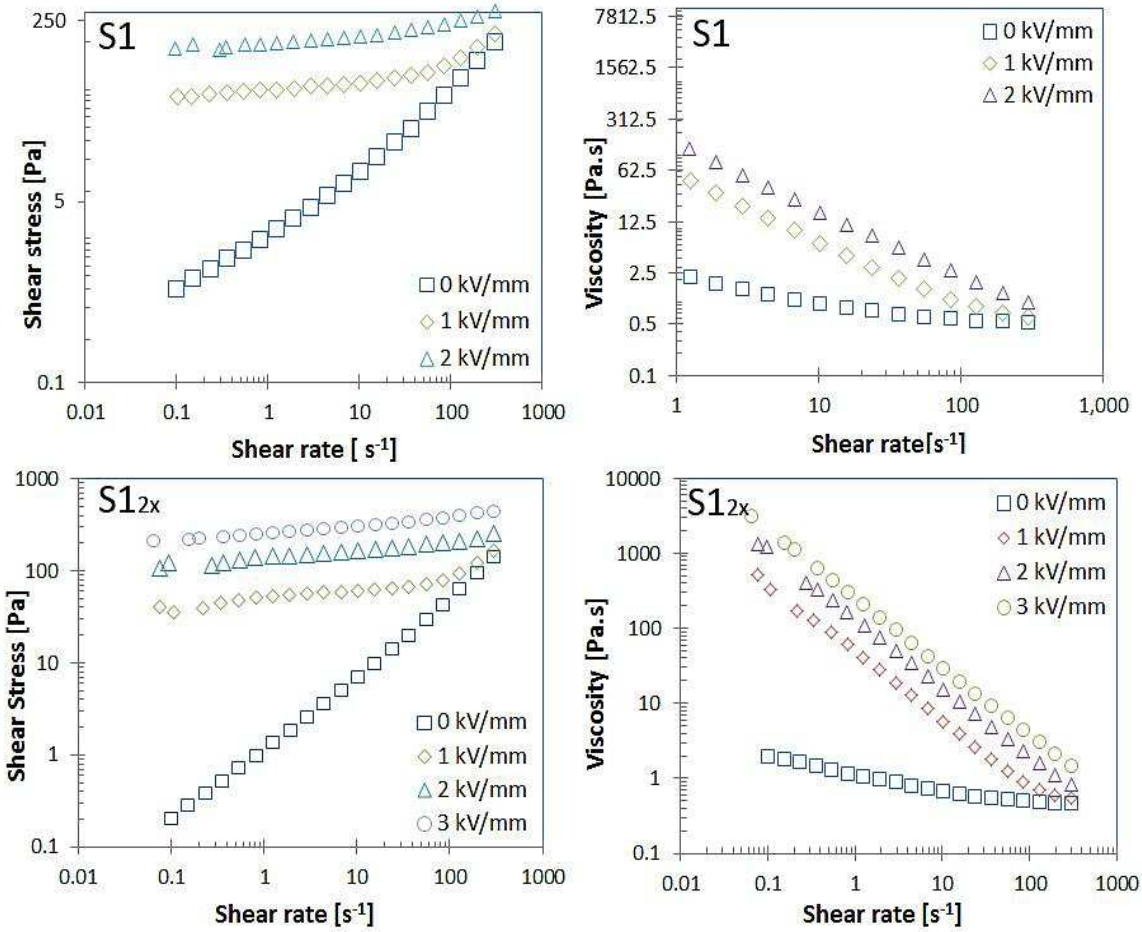

Figure 47: Flow curves (left) and Viscosity curves (right) of and 10 vol. % samples of S1 (top) and $S1_{2x}$ (bottom)

6.4.2 EFFECT OF CHANGE IN PARTICLE VOLUME CONCENTRATION

Figure 48, shows the effect of change of PPy particles volume concentration of sample S1 from 5 vol. % to 10 vol. % on the ER effect. The ER properties of 10 vol. % samples of S2 and S3 were not possible to measure owing to their higher conductivity, which tend to make the system to short-circuit during the rheological measurement.

From the Fig 48, it is evident that the 10 vol. % samples of S1 shows better ER activity with a significant increase in yield stress and viscosity than the 5 vol. % samples. This is the result of strong electrostatic interaction between particles and the increase in number of chain like structures formed by the particles with the increase in PPy content.

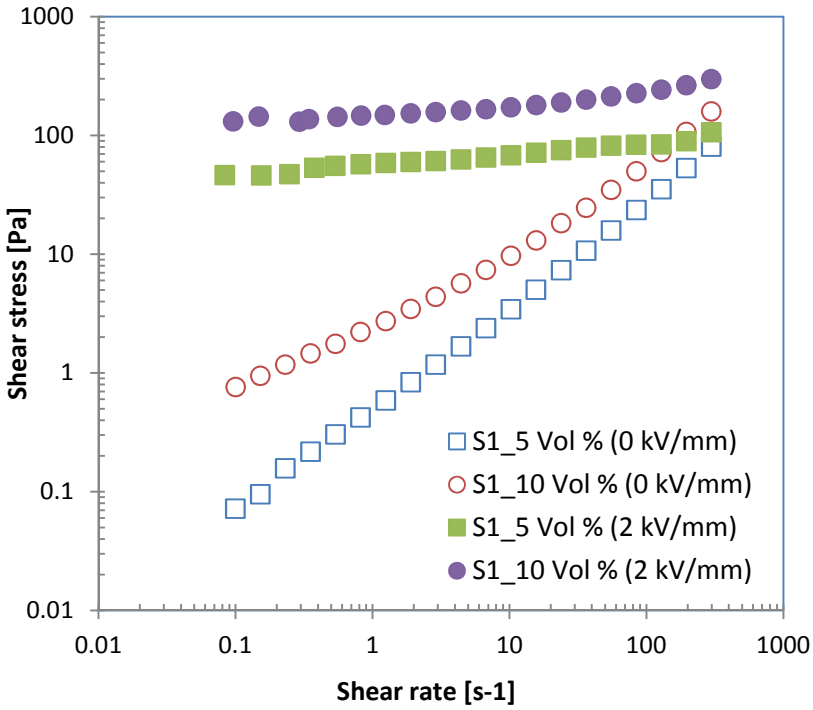

Figure 48: The Flow curve of shear stress as a function of shear rate for 5 and 10 vol. % samples of S1 under different applied electric field strength

6.4.3 DYNAMIC OSCILLATORY EXPERIMENTS

The formation of internal chain-like structure of the polarized particles under the application of electric filed is also accompanied by the change in viscoelastic characteristics. Figure 49 and 50 depict the dependence of *G'* and *G"* on the strain amplitude in oscillatory flow for 5 vol. % samples of S1 and S3.

Without the electric field the viscous modulus the viscous modulus *G"* in the suspension is dominant over elastic modulus *G'*. However, when the electric field is engaged *G'* becomes significantly higher than *G"* in the linear viscoelastic region and both moduli increase rapidly in several orders of magnitude from their electric field-off values.

When the strain acting on the internal structure increases beyond a certain degree, the elastic and viscous moduli intersect each other, at that point the chain structure of the ER fluid breaks rapidly and the system starts to flow.

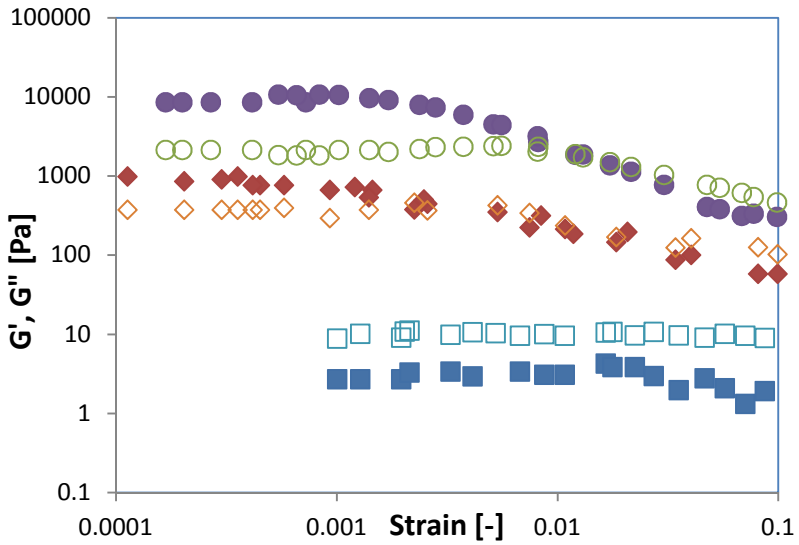

Figure 49: Strain dependence of storage modulus (G', solid symbols) and loss modulus (G", open symbols) for 5 vol. % samples of S1 under various E (kV/mm) 0 (squares), 1 (diamond) and 3 (circles).

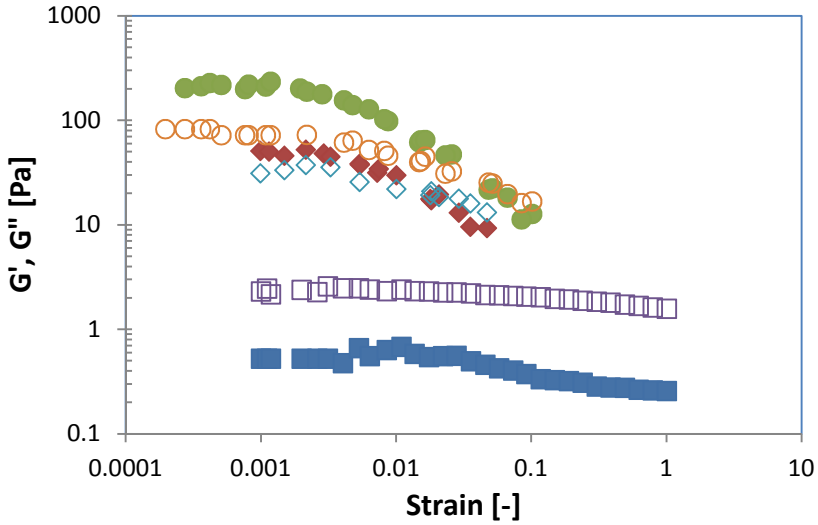

Figure 50 : Strain dependence of storage modulus (G', solid symbols) and loss modulus (G", open symbols) for 5 vol. % samples of S1 under various E (kV/mm) 0 (squares), 0.25 (diamond) and 0.5 (circles).

For practical applications it is essential to know the moduli in linear viscoelastic region and their angular frequency dependence. Figure 50 represents the change in *G'* and *G"* of 5 vol. % sample of S1 and S3 at a small strain of 10^{-4} in the linear viscoelastic region with and without the applied electric field strength.

With increasing electric field strength, values of both moduli increase signifying more established and rigid chain-like structures induced by the applied electric field.

At the low angular frequency region, *G'* is nearly independent of frequency and is larger than *G"* at the same electric field strength due to the predominant elasticity over viscosity.

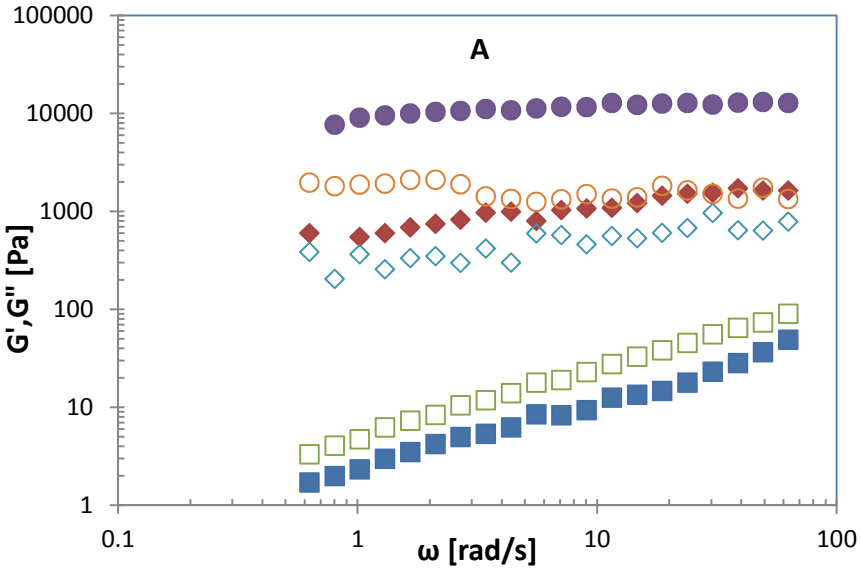

Figure 51 : Angular frequency, ω, dependence of storage modulus, G', (solid symbols) and loss modulus (G", open symbols) for 5 vol. % samples of S1 under various E (kV/mm) 0 (squares), 1 (diamond) and 3 (circles)

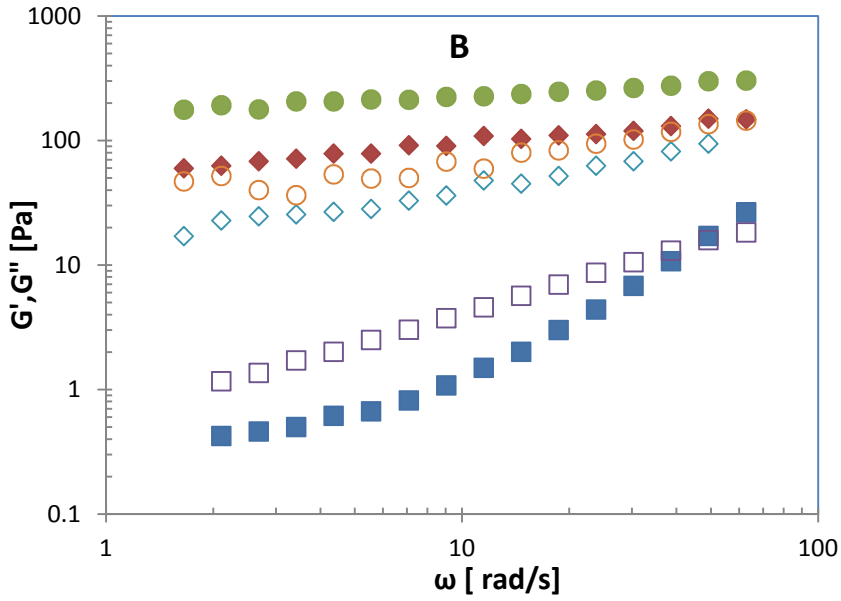

Figure 52 : Angular frequency, ω, dependence of storage modulus, G', (solid symbols) and loss modulus (G", open symbols) for 5 vol. % samples S3 under various E (kV/mm) 0 (squares), 0.25 (diamond) and 0.5 (circles)

6.5 DIELECTRIC MEASUREMENTS

Generally, dielectric properties of ER suspensions are closely connected to the ER effect since the chain-like structure is formed by induced electrostatic interactions between dispersed dielectric particles caused by interfacial polarisation. The dielectric spectra are presented in the Fig 51 and the relaxation times obtained are tabulated below.

Table 4 : Dielectric relaxation time for the prepared samples

Sample	**Relaxation time t_{rel} [s]**
S1	6.95×10^{-5}
$S1_{2x}$	1.46×10^{-4}
S2	3.55×10^{-6}
S3	4.34×10^{-6}

The relaxation time, t_{rel}, which is defined as the reciprocal of frequency at which the dielectric loss factor, ε", is maximum. The value of t_{rel} reflects the rate of interfacial polarization, and is observed to be lower for samples containing Ag (S2 and S3) in comparison to the samples containing pure PPy, which is due to higher induced charges on the interface between the particles.

On the other hand, unfortunately there appears to be a second peak on the dielectric spectra for samples containing Ag, which renders the data can't be fit using the Havriliak-Negami model. This might be due to the electrode polarization of these particles owing to higher conductivity than the neat PPy.

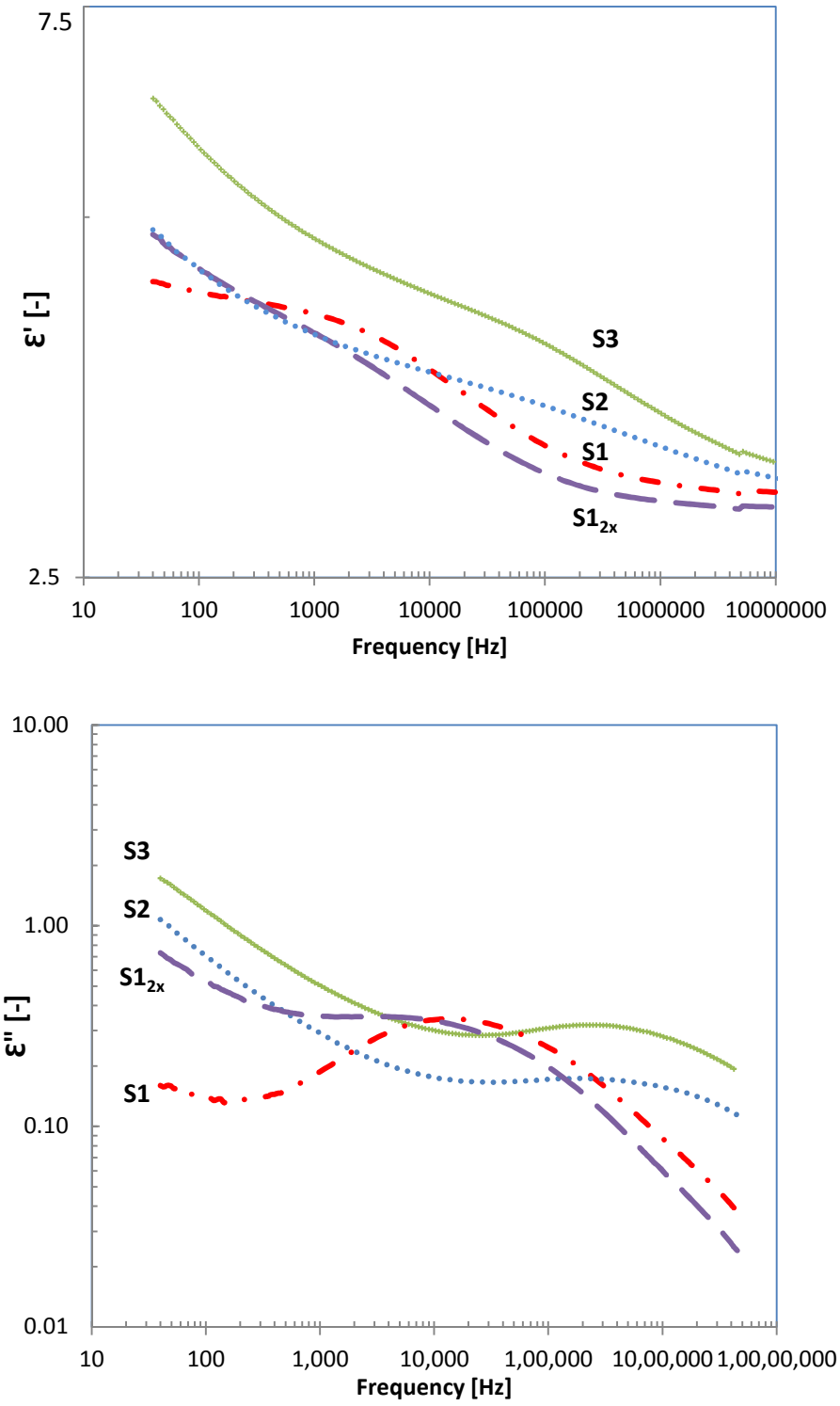

Figure 53: Relative permittivity, ε′ (a) and dielectric loss factor, ε″ (b) as a function of the frequency for 5 vol. % ER suspensions of samples S1, S1$_{2x}$, S2 and S3 in silicone oil at 0.5 kV/mm

CONCLUSION

The PPy and PPy–Ag composite particles were synthesized via oxidation of Py with a mixture of APS and $AgNO_3$ and used as a dispersed phase of a novel ER suspension.

Morphological studies through SEM revealed that PPy particles are globular in shape, and their sizes tend to increase and form agglomerates when $AgNO_3$ is used as an oxidant during the synthesis.

From the FTIR analysis the presence of PPy in the samples were confirmed and it also proved that the increase in $AgNO_3$ during the synthesis has very little effect on the chemical structure of PPy as the characteristic peaks of PPy is observed on FTIR spectra of each sample.

From the TGA measurements the amount of Ag present in the samples was calculated, which also correlates with the density measurements, revealing the amount of Ag increases as the amount of $AgNO_3$ increases during the synthesis of PPy. X-ray diffraction analysis also proved the presence of Ag in those samples. The conductivity of the samples was measured using Van der Paaw four point method, and the results proved that the presence of Ag particles increased their conductivity up to three orders of magnitude.

To obtain insight into the ER activity of prepared ER suspensions, rheological and dielectric properties were evaluated. Although the dielectric measurements revealed that the relaxation time tends to decrease as the amount of Ag increase there by resulting in faster ER response in comparison to that of neat PPy, the rheological measurements showed that the ER suspensions of PPy–Ag composite particles in silicone oil can only be employed as a novel ER suspension, when the applied external electric field strength is not above 0.5 kV/mm, whereas the ER suspension prepared using neat PPy can be employed over a wide range of external electric field strength up to 3 kV/mm. This is due to the higher conductivity of the suspensions containing Ag as found in the conductivity measurements.

BIBLIOGRAPHY

1. SEDLAČÍK, M., MRLÍK, M., PAVLÍNEK, V., SÁHA, P. and QUADRAT, O. Electrorheological properties of suspensions of hollow globular titanium oxide/polypyrrole particles. *Colloid and Polymer Science*. 2011, Vol. 290, no. 1, pp. 41–48.

2. PAPADOPOULOS, Chris A. Brakes and clutches using ER fluids. *Mechatronics*. August 1998, Vol. 8, no. 7, pp. 719–726.

3. CHENG, Q., PAVLINEK, V., Ying, Y., Yanfang, LI, Chunzhong and SAHA, P., Synthesis and electrorheological characteristics of sea urchin-like TiO2 hollow spheres. *Colloid and Polymer Science*. 2011, Vol. 289, no. 7, pp. 799–805.

4. HOU, J., SHI, L., and ZHU, Q. Electrorheological properties and structure of ($BaTiO(C_2O_4)_2/NH_2CONH_2$). *Journal of Solid State Chemistry*. 2006, Vol. 179, no. 6, pp. 1874–1878.

5. KO, Young G., LEE, Hyun J., CHUN, Y., CHOI, U., and YOO, K. Positive and Negative Electrorheological Response of Alginate Salts Dispersed Suspensions under Electric Field. *ACS applied materials & interfaces*. 2013, Vol. 5, no. 3, pp. 1122–30.

6. CHOUGULE, M. a. Synthesis and Characterization of Polypyrrole (PPy) Thin Films. *Soft Nanoscience Letters*. 2011, Vol. 01, no. 01, pp. 6–10.

7. THE NOBEL FOUNDATION. The Nobel Prize in Chemistry 2000-Invention and developement of Conducting Polymers. [online]. [Accessed 28 February 2013]. Available from: http://www.nobelprize.org/nobel_prizes/chemistry/laureates/2000/.

8. SHIRAKAWA, H and LOUIS, EJ. Synthesis of electrically conducting organic polymers: halogen derivatives of polyacetylene (CH)x. *Journal of chemical Society.* 1977, no. 578, pp. 578–580.

9. CHANDRASEKHAR PRASANNA. Conducting Polymer Fundamentals and Applications. Kluwer Academic Publishers, 1999. pp. 1–37. ISBN 0-7923-8564-0.

10. MACDIARMID, Alan G. *Synthetic Metals : A Novel Role for Organic Polymers (Nobel Lecture)*. S.l. 2001.

11. EPSTEIN, AJ. Electrical Conductivity in Conjugated Polymers. *conductive polymers*. 1999, Vol. 7, pp. 1–9.

12. POUGET, J P, OBLAKOWSKI, Z, NOGAMI, Y, ALBOUY, P A, LARIDJANI, M, OH, E J, MIN, Y, MACDIARMID, A G, TSUKAMOTO, J, ISHIGURO, T and EPSTEIN, A J. Recent structural investigations of metallic polymers. *Synthetic Metals*. 1994, Vol. 65, pp. 131–140.

13. STREET, G. B., CLARKE, T. C., GEISS, R. H., LEE, V. Y., NAZZAL, a., PFLUGER, P. and SCOTT, J. C. Characterization of Polypyrrole. *Le Journal de Physique Colloques*.1983, Vol. 44, no. C3, pp. C3–599–C3–606.

14. SAVILLE, Paul. *Polypyrrole Formation and Use- Defence R & D Canada – Atlantic*. Dartmouth. 2005.

15. SABOURAUD, G., SADKI, S., and BRODIE, N., The mechanisms of pyrrole electropolymerization. *Chemical Society Reviews*. 2000, Vol. 29, no. 5, pp. 283–293.

16. BREZOI, Dragos-Viorel. Polypyrrole films prepared by chemical oxidation of pyrrole in aqueous $FeCl_3$ solution. *Journal of Science and Arts*. 2010, Vol. 12, no. 1, pp. 53–58.

17. KANG-JIN KIM*, HYUNG-SOO SONG, Jin-Doo Kim. Mechanism of Electropolymerization of Pyrrole in Acidic Aqueous Solutions. *Bulletin of the Koren Chemical Society*. 1988, Vol. 9, no. 4, pp. 248–251.

18. B.L.FUNT AND A.F. DIAZ. *Organic Electrochemistry: an Introduction and a Guide*. New York: Marcel Dekker, 1991.

19. TAUNK, M., KAPIL, A., and CHAND, S., Hopping and tunneling transport over a wide temperature range in chemically synthesized doped and undoped polypyrrole. *Solid State Communications*. 2010, Vol. 150, no. 37-38, pp. 1766–1769.

20. PRIGODIN, Vladimir N., SAMUKHIN, Alexander N. and EPSTEIN, Arthur J. Variable range hopping in low-dimensional polymer structures. *Synthetic Metals*. 2004, Vol. 141, no. 1-2, pp. 155–164.

21. PAASCH, G, LINDNER, T and SCHEINERT, S. Variable range hopping as possible origin of a universal relation between conductivity and mobility in disordered organic semiconductors. *Synthetic Metals*. 2002, Vol. 132, no. 1, pp. 97–104.

22. TAT'YANA, V and EFIMOV, N. Polypyrrole: a conducting polymer; its synthesis, properties and applications. *Russian chemical reviews*. 2007, Vol. 443.

23. LANGE, U, ROZNYATOVSKAYA, N., and MIRSKY, M. Conducting polymers in chemical sensors and arrays. *Analytica chimica acta*. 2008, Vol. 614, no. 1, pp. 1–26.

24. KURZWEIL, P. Capacitors| Electrochemical Polymer Capacitors. Encyclopedia of Electrochemical Power (ed.), *Encyclopedia of Electrochemical Power Sources*. Amsterdam: Elsevier, 2009. pp. 679–684. ISBN 978-0-444-52745-5.

25. PARK, J. and PARK, O. Hybrid electrochemical capacitors based on polyaniline and activated carbon electrodes. *Journal of Power Sources*. 2002, Vol. 111, no. 1, pp. 185–190.

26. SHIN, S., KIM, J., KIM, Y., and KIM, S., Enhanced performance of organic light-emitting diodes by using hybrid anodes composed of graphene and conducting polymer. *Current Applied Physics*. 2013.

27. UNIVERSITY OF COLORADO. Willis M. Winslow Electrical Engineering Research & Invention. [online]. [Accessed 18 April 2013]. Available from: http://www.colorado.edu/engineering/deaa/cgi-bin/display.pl?id=178.

28. WINSLOW, W.M. Method and means for translating electrical impulses into mechanical force. US Patent 2,417,850. 1947.

29. AKHAVAN, J and SLACK, K. Coating of a semi-conducting polymer for use in electrorheological fluids. *Synthetic Metals*. 2001, Vol. 124, no. 2–3, pp. 363–371.

30. HUANG, Xianxiang, WEN, Weijia, YANG, Shihe and SHENG, Ping. Mechanisms of the giant electrorheological effect. *Solid State Communications*. 2006, Vol. 139, no. 11-12, pp. 581–588.

31. ZHANG, L., KURIYAGAWA, T., KAKU, T., and ZHAO, J. Investigation into electrorheological fluid-assisted polishing. *International Journal of Machine Tools and Manufacture*. 2005, Vol. 45, no. 12-13, pp. 1461–1467.

32. CHENG, Q., PAVLINEK, V., LENGALOVA, A., LI, C., HE, Y., and SAHA, P. Conducting polypyrrole confined in ordered mesoporous silica SBA-15 channels: Preparation and its electrorheology. *Microporous and Mesoporous Materials*. 2006, Vol. 93, no. 1-3, pp. 263–269.

33. KIMURA, H, AIKAWA, K, MASUBUCHI, Y, TAKIMOTO, J, KOYAMA, K and UEMURA, T. `Positive' and `negative' electro-rheological effect of liquid blends. *Journal of Non-Newtonian Fluid Mechanics*. 1998, Vol. 76, no. 1-3, pp. 199–211.

34. HAO, Tian. Chapter 3: The positive, negative, photo-ER, and eleetrolnagnetorheological (EMR) effects. *Electrorheological Fluids: The Non-aqueous Suspensions*. Elsevier, 2005. pp. 83–113. ISBN 9780444521804.

35. PAVLINEK, V, SÁHA, P, QUADRAT, O and STEJSKAL, J. Rheological behavior of poly (methyl methacrylate) dispersions stabilized by a diblock copolymer. 2. Positive and negative electrorheological effect. *Langmuir*. 2000, no. 14, pp. 1447–1449.

36. AKHAVAN, J. Electro-rheological polymers. *Proceedings of the Institution of Mechanical Engineers, Part G: Journal of Aerospace Engineering*. 2007, Vol. 221, no. 4, pp. 577–587.

37. KLINGENBERG, D. J. Introduction to Electrorheology and Magnetorheology. [online]. [Accessed 22 March 2013]. Available from: http://homepages.cae.wisc.edu/~klingen/group/ermrintro.htm

38. HAO, T., Electrorheological suspensions. *Advances in Colloid and Interface Science*. 29 March 2002, Vol. 97, no. 1-3, pp. 1–35.

39. FOSSUM, J. O, MÉHEUST, Y, PARMAR, K. P. S, KNUDSEN, K. D, MÅLØY, K. J and FONSECA, D. M. Intercalation-enhanced electric polarization and chain formation of nano-layered particles. *Europhysics Letters (EPL)*. 2006, Vol. 74, no. 3, pp. 438–444.

40. BOISSY, C, ATTEN, P. and FOULC, J.-N. On a negative electrorheological effect. *Journal of Electrostatics*. July 1995, Vol. 35, no. 1, pp. 13–20.

41. CETIN, B, UNAL, H I and EROL, O. The negative and positive electrorheological behavior and vibration damping characteristics of colemanite and polyindene / colemanite conducting composite. *Smart Materials and Structures*. 2012, Vol. 21, no. 12, pp. 125011.

42. WU, C. W. Negative electrorheological effect and electrical properties of a Teflon/silicone oil suspension. *Journal of Rheology*. 1997, Vol. 41, no. 2, pp. 267.

43. KOMODA, Y, SAKAI, N, RAO, TN, TRYK, DA and FUJISHIMA, A. Photoelectrorheological phenomena involving TiO_2 particle suspensions. *Langmuir*. 1998, Vol. 7463, no. 16, pp. 1081–1091.

44. BOSSIS, G, VOLKOVA, O, LACIS, S and MEUNIER, A. Magnetorheology: Fluids, Structures and Rheology. ODENBACH, Stefan (ed.), *Ferrofluids*. Berlin, Heidelberg: Springer Berlin Heidelberg, 2003. pp. 202–230.

45. KLINGENBERG, Daniel J. Magnetorheology: Applications and challenges. *AIChE Journal*. February 2001, Vol. 47, no. 2, pp. 246–249.

46. STANWAY, R. Smart fluids: current and future developments. *Materials Science and Technology*. 2004, Vol. 20, no. 8, pp. 931–939.

47. WEN, W. and SHENG, P. Two-and three-dimensional ordered structures formed by electro - magnetorheological colloids. *Physica B: Condensed Matter*. 2003, Vol. 338, no. 1-4, pp. 343–346.

48. HAO, Tian. Chapter 5: Critical parameters to the electrorheological effect. *Electrorheological Fluids: The Non-aqueous Suspensions*. S.l.: Elsevier, 2005. pp. 152–234.

49. YILMAZ, H., ZENGIN, H., and UNAL, H., Synthesis and electrorheological properties of polyaniline / silicon dioxide composites. *Journal of Materials Science*. 2012, Vol. 47, no. 13, pp. 5276–5286.

50. YIN, J., XIA, X., XIANG, L., and ZHAO, X., Temperature effect of electrorheological fluids based on polyaniline derived carbonaceous nanotubes. *Smart Materials and Structures*. 2011, Vol. 20, no. 1, pp. 015002.

51. HAO, T., Chapter 10: Applications of electrorheological fluids. *Electrorheological Fluids: The Non-aqueous Suspensions*. Elsevier, 2005. pp. 518–551. ISBN 1383-7303.

52. NGUYEN, Q. H., CHOI, S. B., and PARK, Y. G. An analytical approach to optimally design of electrorheological fluid damper for vehicle suspension system. *Meccanica*. 2012, Vol. 47, no. 7, pp. 1633–1647.

53. KAMELREITER, M., KEMMETMÜLLER, W., and KUGI, A., Digitally controlled electrorheological valves and their application in vehicle dampers. *Mechatronics*. 2012, Vol. 22, no. 5, pp. 629–638.

54. RABINOW, J., Smart Fluids Move into the Marketplace. *Industrial Physicist*. 2003, pp. 14–17.

55. SUN, T., HUANG, Z., and CHEN, D., Signal frequency-based semi-active fuzzy control for two-stage vibration isolation system. *Journal of Sound and Vibration*. 2005, Vol. 280, no. 3-5, pp. 965–981.

56. FURUSHO, J., SAKAGUCHI, M., TAKESUE, N. and KOYANAGI, K. Development of ER Brake and its Application to Passive Force Display. *Journal of Intelligent Material Systems and Structures*. 2002, Vol. 13, no. 7-8, pp. 425–429.

57. MADEJA, J., KESY, Z., and KESY, A., Application of electrorheological fluid in a hydrodynamic clutch. *Smart Materials and Structures*. 2011, Vol. 20, no. 10, pp. 105005.

58. KIM, W.B., MIN, B.-K. and LEE, S.J. Development of a padless ultraprecision polishing method using electrorheological fluid. *Journal of Materials Processing Technology*. 2004, Vol. 155-156, pp. 1293–1299.

59. AKROD v2 - Active Knee Rehabilitation Device. [online]. [Accessed 16 April 2013]. Available from:
http://www.technovelgy.com/ct/Science-Fiction-News.asp?NewsNum=455

60. INNOVENT TECHOLOGIEENTWICKLUNG. Magnetorheological fluids. [online]. [Accessed 26 February 2013]. Available from: http://www.innovent-jena.de/en/INNOVENT/Departments/Magnetic-and-optical-systems/Magnetic_Materiales/Magnetorheological-fluids__4690/

61. GOZDALIK, A., WYCISLIK, H., and PLOCHARSKI, J., Electrorheological effect in suspensions of polyaniline. *Synthetic metals*. 2000, Vol. 109, pp. 147–150.

62. OTSUBO, Y. Electrorheological properties of silica suspensions. *Journal of Rheology*. April 1992, Vol. 36, no. 3, pp. 479.

LIST OF ABBREVIATIONS

PPy	Polypyrrole
Ag	Silver
ER	Electrorheology
TiO_2	Titanium dioxide
$BaTiO_2$	Barium Titanium dioxide
CP	Conductive polymers
Na	Sodium
K	Potassium
Li	Lithium
Ca	Calcium
PF_6	Hexafluorophosphate
BF_4	Boron tetrafluoride
AsF_6	Arsenic hexafluoride
$FeCl_3$	Ferric chloride
$K_2S_2O_8$	Potassium per sulphate
APS	Ammonium persulfate
Py	Pyrrole
eV	Electron Volt
Scm^{-1}	siemens per metre
kV/mm	Kilovolt per millimetre
Pa.s	Pascal second
Vol. %	Volume percentage
E	Electric field strength
PMMA	Polymethyl methacrylate

τ	Shear stress [tow]
η	Viscosity [eta]
MR	Magnetorheology
ρ	Density
C	Concentration
Hz	Frequency
PANI	Polyaniline
SDO	Silicon dioxide
SEM	Scanning electron microscope
TGA	Thermogravimetric analysis
DC	Direct current
CSR	Controlled shear rate mode
LVR	Linear viscoelastic region
µm	Micrometre
Wt. %	Weight percentage
$\dot{\gamma}$	Shear rate
G'	Viscous modulus / loss modulus
G"	Elastic modulus/ Storage modulus
$\mathcal{E}'$	Relative permittivity
$\mathcal{E}''$	Dielectric loss factor

LIST OF FIGURES

Figure 1: Structure of most common CPs and their abbreviations [9]. 12

Figure 2: Illustration of the oxidative doping (p-doping) of Leucoemeraldine base and Emeraldine base results in the conductive Emeraldine salt [11]. 13

Figure 3: Structure of Polypyrrole [14]. 14

Figure 4: Oxidative polymerization of Py to PPy proceeds via the formation of a Py radical cation, which subsequently couples with another radical cation to form the Py dimer. This Process is then repeated to form longer chains [14]. 15

Figure 5: Illustration of the structures of neutral (Aromatic/quinoid) and the charged polaron/ bipolaron forms of polypyrrole [14] 16

Figure 6 : Effect of monomer to oxidizing agent on the conductivity and yield. Note that the conductivity drops above the 1:1 molar ratio [19] 17

Figure 7: Change in viscosity of 10 wt. % PPy–SBA-15 particles in silicone oil at different applied electric field strengths [32]. 20

Figure 8: Change in Shear stress of 10 wt. % PPy-SBA-15 particles in silicone oil at different electric field strengths [32]. 20

Figure 9: Suspension of dielectric particles (2 vol. %) in silicone oil, (A) The scattered random dispersed phase. (B) Formation of fibrous structures perpendicular to the field (The direction of the external field is indicated by the arrow)[33]. 21

Figure 10: Change in shear stress of a positive ER suspension depending on the applied electric filed strength in kV/mm (indicated by the numbers on the each step (34) 22

Figure 11 : Schematic illustration of the formation dipoles and the resulting fibrous structures (head-to-tail configuration) perpendicular to the electric field [38]. 22

Figure 12: Illustration of (a) phase separation in the dispersion (b) Quincke rotation [41] 23

Figure 13: A- Negative ER effect and B- Positive ER effect. Note that the viscosity increases for A and decreases for B with respect to the increase in applied external electric field strength [[34] 24

Figure 14: Formation of fibrillated particle structure under the magnetic field (60) 25

Figure 15: Dependence of the shear stress of ER fluid (PANi/Silicone oil) on the electric filed strength (61)..... 27
Figure 16: The change in yield stress of silica/silicone oil ER system against the product of the square of applied electric field and the particle volume fraction (62) 27
Figure 17: Decrease in apparent viscosity of the Silica/Silicone oil ER system with respect to the increase in frequency of the field [38] 28
Figure 18 : Effect of change in concentration of particles on the ER properties of PANi in silicone oil and PANi in SiO_2 (SDO)..... 29
Figure 19: Negative Effect of Temperature on Shear stress of PANI/Silicone di oxide and PANi/Silicone oil ($\dot{\gamma}$ = 1.0 s^{-1}, 20 wt. %) [49]...... 30
Figure 20: Flow curve of shear stress versus shear rate under zero electric field for the 10 vol%. PANi-CT suspension at different temperatures [50]. 31
Figure 21: Flow curve of shear stress versus shear rate under electric field (E= 3kV/mm) for the 10 vol. % PANi-CT suspension at different temperatures [50]. 32
Figure 22: Schematic configuration of the bypass type ER damper (55)..... 34
Figure 23: Damping force versus piston velocity at various voltages [56] 35
Figure 24: Arrangement of a hydrodynamic clutch with ER/MR fluid: P—pump with mixed through-flow, T_I—first section of turbine with axial flow, T_{II}—second section of turbine with mixed through-flow, 1—wedge shape blade, 2—inside housing wall, 3—outside housing wall (57) 36
Figure 25: The principle of ER fluid assisted material removal [58] 37
Figure 26: AKROD Electro-Rheological Fluid knee Joint [59]. 38
Figure 27: Apparatus used for the preparation of PPy particles..... 42
Figure 28 Temperature of the reaction mixture (PPy-APS/$AgNO_3$) over time 43
Figure 29: SEM micrograph of Sample S1..... 46
Figure 30: SEM micrograph of Sample S2..... 47
Figure 31: SEM micrograph of Sample S3..... 47
Figure 32: SEM micrograph of Sample S4..... 48
Figure 33: SEM micrograph of Sample S5..... 48
Figure 34: FTIR spectra of prepared samples 49
Figure 35: XRD pattern of S3 confirms the presence of Ag 51

Figure 36: Thermograms of prepared samples indicating the amount of PPy present in each of them 52

Figure 37 : Dependence of shear stress (τ), on shear rate ($\dot{\gamma}$), for 5 vol. % sample of S1 at various electric field strengths E (kV/mm) 53

Figure 38: Dependence of shear stress (τ), on shear rate ($\dot{\gamma}$), for 5 vol. % sample of $S1_{2x}$ at various electric field strengths E (kV/mm) 53

Figure 39 : Dependence of shear stress (τ), on shear rate ($\dot{\gamma}$), for 5 vol. % sample of S2 at various electric field strengths E (kV/mm) 54

Figure 40: Dependence of shear stress (τ), on shear rate ($\dot{\gamma}$), for 5 vol. % sample of S3 at various electric field strengths E (kV/mm) 54

Figure 41: Flow curves of shear stress (τ) as a function of shear rate ($\dot{\gamma}$) for the 5 vol. % ER fluids of S1, S2 and S3 at 0.3 kV/mm 56

Figure 42: Dependence of shear viscosity (□) on shear rate ($\dot{\gamma}$) for 5 vol. % sample of S1 at various electric field strengths E (kV/mm) 57

Figure 43: Dependence of shear viscosity (□) on shear rate ($\dot{\gamma}$) for 5 vol. % sample of $S1_{2x}$ at various electric field strengths E (kV/mm)..... 57

Figure 44 : Dependence of shear viscosity (□) on shear rate ($\dot{\gamma}$) for 5 vol. % sample of S2 at various electric field strengths E (kV/mm) 58

Figure 45: Dependence of shear viscosity (□) on shear rate ($\dot{\gamma}$) for 5 vol. % sample of S3 at various electric field strengths E (kV/mm) 58

Figure 46: Flow curve (A) and Viscosity curve (B) of 5 vol. % Samples of S1 and $S1_{2X}$ at 0 and 3 kV/mm of applied electric field strength 59

Figure 47: Flow curves (left) and Viscosity curves (right) of and 10 vol. % samples of 60

Figure 48: The Flow curve of shear stress as a function of shear rate for 5 and 10 vol. % samples of S1 under different applied electric field strength 61

Figure 49: Strain dependence of storage modulus (G', solid symbols) and loss modulus (G", open symbols) for 5 vol. % samples of S1 under various E (kV/mm) 0 (squares), 1 (diamond) and 3 (circles)...... 62

Figure 50 : Strain dependence of storage modulus (G', solid symbols) and loss modulus (G", open symbols) for 5 vol. % samples of S1 under various E (kV/mm) 0 (squares), 0.25 (diamond) and 0.5 (circles)...... 62

Figure 51 : Angular frequency, ω, dependence of elastic modulus, G', (solid symbols) and viscous modulus (G", open symbols) for 5 vol. % samples of S1 under various E (kV/mm) 0 (squares), 1 (diamond) and 3 (circles)..... 63

Figure 52 : Angular frequency, ω, dependence of elastic modulus, G', (solid symbols) and viscous modulus (G", open symbols) for 5 vol. % samples S3 under various E (kV/mm) 0 (squares), 0.25 (diamond) and 0.5 (circles) 63

Figure 53: Relative permittivity, ε′ (a) and dielectric loss factor, ε″ (b) as a function of the frequency for 5 vol. % ER suspensions of samples S1, $S1_{2x}$, S2 and S3 in silicone oil at 0.5 kV/mm..... 65

LIST OF TABLES

Table 1: Composition of reaction mixtures *41*

Table 2: The molar concentrations of oxidants APS and $Ag.NO_3$ (C) used for the synthesis of particles employed in ER fluids and their density (ρ), amount of Ag (w_{Ag}) *50*

Table 3: Yield stress of prepared samples at $\dot{\gamma}$ = 0.1 s^{-1} and E= 0.3 kV/mm *55*

Table 4 : Dielectric relaxation time for the prepared samples *64*